THE CORROSION RESISTANCE OF CARBON-CONTAINING

OXIDE REFRACTORIES IN MELTS

A Thesis submitted for the degree of

MASTER OF PHILOSOPHY

of the

University of London

by

HAN KYOU PARK, B.Eng.

Department of Chemical Engineering

and Chemical Technology,

Imperial College of Science and Technology,

London, S.W.7.

February, 1972.

Abstract

An account is given of experiments about the rate of
dissolution of carbon-containing oxide refractories in melts.
Much is known about the dissolution of oxides, but not about
composites ; so components e.g. oxide and carbon were first
studied separately.   Carbon was oxidized in an air stream and
under melts under conditions of natural convection.   The disso-
lution of the composite refractories under melts, simulating the
conditions in oxygen steelmaking, was measured.

The rate controlling process of carbon-containing alumina
in sodium tetraborate in oxygen free N_2 atmosphere, where no
destructive oxidation of carbon was involved, was found to be
the same as alumina a diffusion controlled process. The initial
corrosion rate of carbon-containing alumina reduced with the in-
creased carbon content.   The steady state corrosion rate was the
same as alumina itself if the pores were poorly filled with car-.
bon.   The reverse effect of porosity occured.   However, the rate
of corrosion of carbon-containing alumina was reduced when the
pores are filled efficiently with carbon.   In this respect, carbon
deposited from resin performed better than carbon formed from
pitch.

The rate of corrosion of carbon-containing alumina in sodium
metavanadate, where a chemical-reaction mechanism prevailed, was
increased compared to corresponding porous alumina.   The reason
for this may be due to the vigorous oxidation of carbon in $NaVO_3$
in oxygen-free atmosphere.

The oxidation of carbon under $NaVO_3$, $Na_2B_4O_7$ and Na_2SiO_3

has been investigated. The equality of the activation energy in each melt suggested the rate determining process was the same. The rate controlling process suggested is a diffusion controlled process, possibly by carbonate anions, diffusing through a carbonate rich superficial layer at the carbon surface.

The work is dedicated to my parents

Mr. & Mrs. Park (Kim),

for their belief in the value of

learning,   for their continuous

encouragement and for financial

support

Acknowledgements

The author wishes to express his sincere gratitude to Mr. L.R. Barrett for his supervision, guidance and encouragement throughout the course of the work. The author is grateful to Professor A.R. Ubbelohde, CBE., FRS., for permitting him to work in his Department.

The author would also like to thank his fellow students in the laboratory for their valuable discussions and to the workshop staff for their help in constructing apparatus.

Thanks are due to the following persons : -

Dr. J.A. Sharp of the Coal Tar Research Association
for providing pitch.

Mr. W. Johnson of The Royal Aircraft Establishment
for providing "Cascote" resin.

Dr. H.C. Kim of Aeronautic Department, Imperial College
for his help in preparation of
optical micrographs.

Mr. L. Moulder for the preparation of the photographs.

Miss M. Ming for the typing.

The author is also indebted to numerous people who encouraged him in one way or another while he was at Imperial College, London.

Contents

Chapter 1 - Introduction

Hitherto, little attention have been paid to the mechanism of dissolution of non-oxide refractories in melts. Non-oxides of interest are carbides, nitrides and borides. Among these, attention was directed to silicon nitride which has attracted attention recently in industry.

It was found difficult to procure the necessary quantities of non-oxide refractories as only small quantities are yet produced commercially ; accordingly preliminary work was started on carbon.

At this time too, it was known that large quantities of carbon impregnated basic refractories were being used in the steel-making industry; also for many years plumbago crucible have been used and recently this material has been under trial as a blast-furnace lining. Therefore, it was accordingly decided to study the mechanism of corrosion of carbon-containing refractory oxides in melts.

In recent years much effort has been made to examine the value of carbon added in small quantities (about 3% - 5%) in practical refractories when attacked by slags. However little work has been undertaken to investigate the corrosion resistance of carbon-containing refractory oxides in melts in order to understand the problem by a quantitative approach. This work was, therefore, undertaken.

Oxide chosen for the research were alumina, magnesia and silica. The technique used for following dissolution was found incompatible with porous silica and magnesia. The reasons were respectively due to the cracking of divitrified silica glass and the solution of magnesia in the dilute acid in the procedure. This can in general be overcome by using the continuous weighing

technique in latter case, but again gases evolved from the specimen would cause irregular movements of the balance beam. So, only alumina remained as a suitable oxide.

Melts chosen were sodium borate and sodium vanadate which were known as corrosive agents. Also corrosion of alumina in these melts was known to occur in two distinct ways, namely by a diffusion controlled process and by a chemical-reaction controlled process, respectively.

Chapter 2

Current understanding of slag attack on carbon-containing oxide refractories.

Chapter 2 Current understanding of slag attack on carbon-

containing refractories

The mechanism of refractory corrosion in melts has been reviewed many times in detail (2) (11) (30) (33). Hence attention will be paid, in this chapter, to the corrosion resistance of carbon-containing refractories, with particular reference to the effect of carbon.

2-1 General remarks

In recent years, as a result of poor performance of non carbon-containing refractories for linings in the basic oxygen-blown steel making process, these are replaced by carbon (pitch) -containing basic refractories.

It is stated (23) that the history of pitch-bearing refractories, which are used in basic bessemers, goes back to the late 19th century. More refined demonstration of performance of this kind of refractory (plumbago bricks) was reported by Dodd and Green (9) as early as 1939. The above authors noticed that the plumbago bricks had eroded only 1 in. after ten casts while the surrounding firebricks had worn back a distance of 4-5 in. Also reported was the notification of the high refractories -under -load and the low, uniform permeability of the plumbago bricks.

It is now understood that carbon deposited from pitch (tar) improves the corrosion resistance of the refractories by slag attack. Hence this chapter will deal with present understanding of the effect of carbon when oxide refractories are attacked by slag.

A recent review article by Kappmeyer and Hubble (23) covers this grounds which helped the present survey considerably.

2-2 Practical carbon-bearing basic refractories

The source of carbon for impregnating basic refractories made from one or more of the various periclase, magnesite and dolomite grains, is pitch (tar) which is a by-product of distillation of coal.

The pitch is introduced into the brick either by blending hot pitch with the refractory raw materials at the point of pressing, while it is at a temperature above the softening point of pitch (pitch-bonded brick) or by impregnating molten pitch into the open pores of pre-sintered brick (pitch-impregnated brick).

Pitch-bonded bricks, when pressed into the shapes, are either cooled for storage or tempered commonly at 450 - 600°F to improve some of the brick characteristics, i.e. to increase low temperature hot strength - this increase in strength reduces possible failure of the lining during burn in, and to improve the resistance of the brick to hydration. Hence pitch in the brick is utilized in three ways ; (1) first it provides a bond for the brick to be handled (2) it protects from hydration (3) it deposits carbon after the heat treatment.

Pitch-impregnated bricks are commonly produced by using a vacuum - pressure technique to impregnate molten pitch into the pores efficiently rather than a simple dipping technique into molten pitch. This technique is basically similar to the method used in the present research. The detail is described in section 3-2-2.

In either brick produced by the procedure described above, carbon is just left in the pores as a type of filler on coking. No evidence is offered that the carbon does bond with the refractory grain (23).

It is worth noting that some of the brick properties are improved by the addition of carbon, i.e. hot strength (21), uniform permeability (9), resistance to spalling. But above all, principal advantage in adding carbon is to minimize slag attack.

2-3 Effect of carbon on slag attack

Kappmeyer and Hubble report that the corrosion resistance of carbon-containing refractories is 2 to 3 times better than that of refractories with-out carbon. This is achieved by the carbon present in the pores on carbonization, as it reduces slag penetration into the pores. However, there are several views on what way slag penetration is inhibited.

2-3-1 Reduction of Fe_2O_3 to metallic iron

Chesters (6) proposed as a possible mechanism that the carbon reduces ferric oxide (or calcium ferrite) to FeO or even metallic iron which has no effect on basic refractories. White (42) also suggested that carbon would stop iron oxide attacking the brick for a similar reason. Recently, Barthel (5) proposed from his miscroscopic examination of worn carbon-bearing refractories that the reduction of penetrated metal ions and solidification of the remaining oxide liquid results in reduced slag attack, if the ratio of CaO/ $(P_2O_5 + SiO_2)$ in the slag is high. If the ratio is low, then the effect is largely physical, i.e. by non-wetting characteristics of graphite.

2-3-2 Reduction of MgO

Robinson (32) proposed that carbon monoxide gas generated by the reaction within the brick may delay the entry of the liquid.

Although he did not specify what reaction produces CO gas in detail, this speculation was supported recently by Pickering and Batchelor (29). The above authors demonstrated experimentally the fundumental incompatibility of the carbon and magnesia in the lining at steel making termperature (1,600°C). The weight losses of carbon-containing magnesia were detected above 1,500°C which was accompanied with the strength losses. This fact convinced them that carbon is lost in this way from the composite carbon/magnesia refractories and the vapour pressure arising from the reaction may help to inhibit slag penetration.

2-3-3 Non-wetting characteristics of carbon

When a liquid drop is in contact with a solid, the contact angle (θ) measures the wetting characteristics of a solid by a liquid. In general, it could be said that a refractory is wetted by slag when the contact angle is smaller than 90°. In this instance, penetration of slag into the pores of refractory is expected. If the contact angle is larger than 90°, the wetting is said not to occur. If θ is approches to zero when a refractory is corroding in slag, the solubility of refractory is expected to be greater and at its maximum (8). Towers (38) appreciated that a higher contact angle and a higher interfacial energy essentially effects to reduce the corrosion of a refractory.

As is well known, carbon shows a large contact angle with a liquid (8). From this consideration, Barthel (4) proposed that carbon in the pores inhibited physically (i.e. due to non-wetting characteristics of carbon) further slag penetration. Herron, Beechan and Padfield (16) also considered that carbon

prevents slag penetration due to lack of wetting between the

carbon and the liquid slag from their microscopic examination

of the test samples subjected to a slag. They varied the

content of carbon in the basic refractories and observed that

the penetration of slag stopped immediately where 3% by weight

or more of carbon present, but the penetration occured when

the carbon content fell below 3% by weight in the test specimens.

2-3-4 Overall effect

As discussed above, carbon reduces slag penetration into

the pores by one or a combination of the several factors considered.

Hence a diminished corrosion within the pores prevents structural

spalling, i.e. erosion of large grains, which is often encountered

with the refractories without carbon.   In other words, the refrac-

tory containing carbon normally wears uniformly compare to the

non carbon-bearing refractory.

Ohba, Ikenoue and Nishikawa (27) noticed from the obser-

vation of tar-bonded brick after service, that a decarburized zone

of 2mm. was formed at the hot face.   Then slag penetration takes

place within this zone and corrosion occurs at a faster rate. Thus,

they concluded that the wear rate is determined by the forming rate

of the decarburized zone.

2-4 Residual carbon content

It is reported (16) that the 3% by weight of retained car-

bon is required to minimize the slag penetration.   Further additon

of carbon did not help to inhibit further slag penetration. Another

noteworthy effect observed by Kappmeyer and Hubble (23) is that an

even higher residual carbon content obtained by other than conventional

procedure (described in section 2-2), i.e. carbon or graphite additions

and precoking of the grains coated with pitch, etc., has shown poor

performance on slag attack. In this connection, however, the pre-

sent work indicated that carbon introduced from resin performed

better than carbon deposited from pitch. The detail is described

in section 7-2-4.

2-5 Structure of carbon deposited in the pores

In general, the formation of carbon particles within the

pores is directly related to the structure of pores (21). The

shape and size of carbon deposited would be either a large, coarse

crystallites formed randomly in a large pores or a fine crystallites

distributed uniformly in a small pores. Recent work by Herron and

Runk (17) indicated that the latter type of carbon formed performs

better with respect to the slag infiltration. Also observed by

them was that when the carbon was distributed uniformly for a fine

particles, not so much carbon (less than 3% by weight) is required

to minimize the slag penetration.

2-6 Properties of carbon-bearing basic refractories related to

corrosion

A laboratory slag test (21) employing real carbon-containing

basic bricks has shown that the composition of refractory exerts

significant influence on corrosion resistance. At present, oxide

refractories used for linings in oxygen-blown steel making processes

are made from periclase, magnesite and dolomite. Hubble (20)

reports that the refractories containing higher magnesia generally

exhibit better corrosion resistance on slag attack. The reason

is that the higher MgO brick contains less CaO which is easily

attacked by iron oxide to form low melting compound calcium

ferrite. It is also reported (23) that burned-impregnated

brick show better corrosion resistance than pitch-bonded brick

at the same MgO level. However, recent work by Herron and

Runk (17) indicated that the pitch-bonded (or tempered) brick

performed better than impregnated brick. The reason suggested

was that the carbon formed in a tempered brick was evenly well

distributed for a fine particles, having better resistance to

the slag penetration compared to the carbon formed in the pores

of impreganated brick.

In view of the erosive action of moving slag encountered

during the steel-making process, hot strength of the refractories

is another important property. The hot strength of periclase

brick is, in general, related to the ratio of CaO / SiO_2 and the

impurities such as Al_2O_3 and Fe_2O_3. High hot strengths are

obtained when the CaO/SiO_2 ratio is increased (13). But Al_2O_3

and Fe_2O_3 should be kept to a minimum, which reduces the $CaO/$

SiO_2 ratio. The reader will find a good account of the whole

subject by Ford (14). As briefly mentioned earlier, the hot

strength of brick is improved by the impregnation of carbon.

This is because the carbon hinders liquid movement at working

temperature.

Another important property is the density of refractories

which will yield better performance when it is at maximum density.

Chapter 3

Preparation and properties of carbon-containing oxide test pieces.

3-1   Sintering of carbon-containing oxide pellets.

3-1-1 Materials used

3-1-2 Moulding

3-1-3 Measurement of volume shrinkage

3-1-4 Operation of experiments

3-1-5 Temperature measurement

3-1-6 The observations made and results obtained

3-2   Impregnation of porous oxide refractories with carbon-containing substances followed by carbonization.

3-2-1 Materials used

3-2-2 Methods of impregnation

3-2-3 Carbonization

Chapter 3   Preparation and properties of carbon-containing oxide
test pieces.

Since carbon has to be put into the texture of ceramics for
the corrosion experiments, two methods of performing this have been
used (1) sintering of mixed carbon plus oxide compacts in an nitrogen
or vacuum   (2) impregnation of porous oxide ceramics with carbon-
containing substances followed by carbonization.

The detailed experimental technique, observations made and
results obtained follow.

3-1 Sintering of carbon-containing oxide pellets

3-1-1 Materials used

Alumina

Analytical reagent quality alumina was ground in a mechanical
agate mortar for four hours to obtain the average particle size of
about five microns. Particle size distribution by the Coulter Counter
is given in Figure 3-1.

Carbon

From the sintering point of view, it is considered better that
the carbon particle size should be small, to assist the alumina in
sintering to grip it and also to prevent cracking whilst it cools
down due to different thermal expansion coefficient of carbon and
alumina.   But from the slag resistance point of view, larger carbon
particle size would be expected to be better to prevent penetration
of slag into porous ceramics when the composite pellet is in contact
with slag.   Also larger carbon particles will have a longer life under
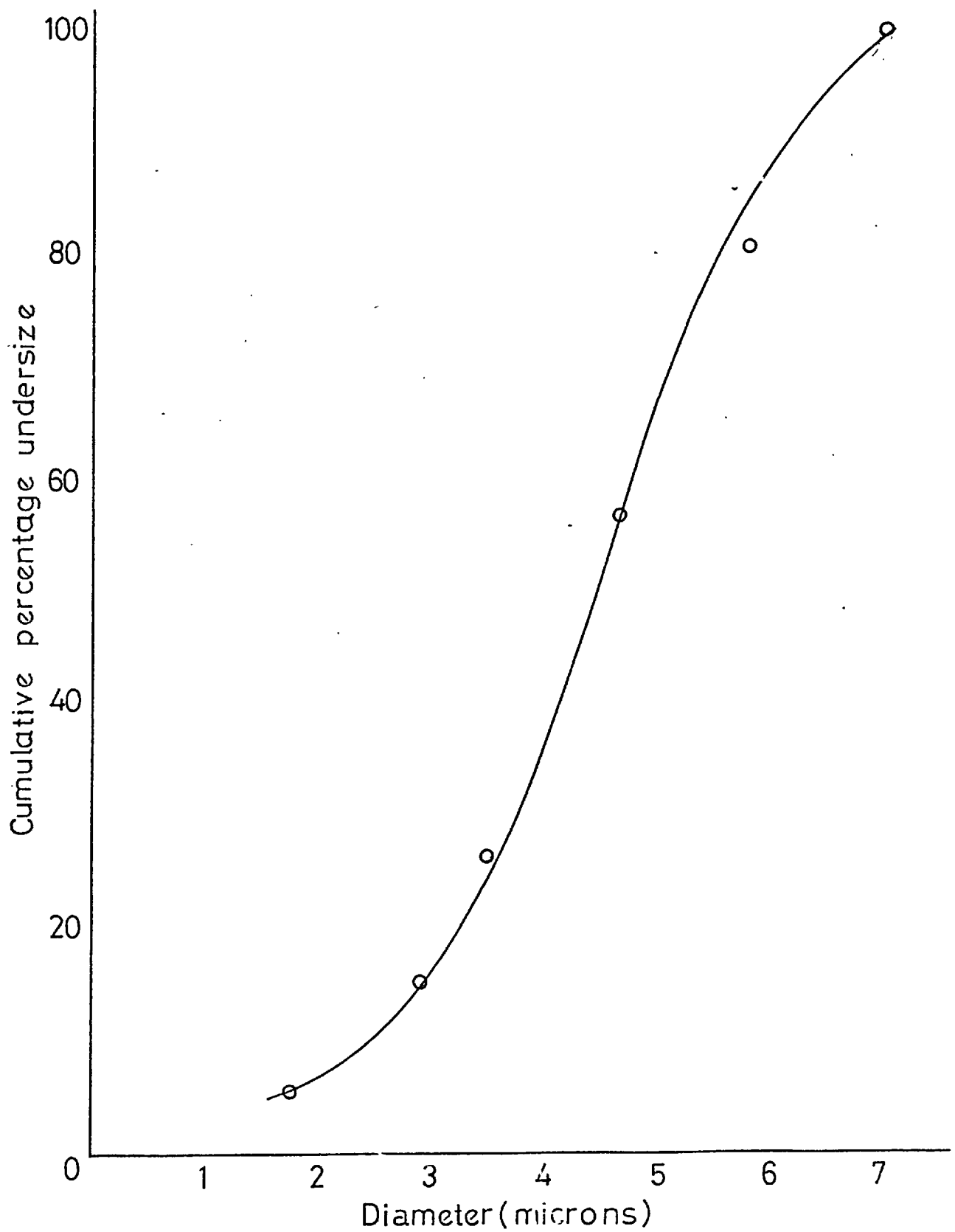oxidizing conditions.

Figure3-1. Particle size distribution of alumina powder.

After some preliminary trials of other sizes, a carbon particle size ranging - 200 + 350 mesh (44 to 76 microns) was adopted.

The form of carbon chosen was grahitized carbon (EY9) to minimise the structural change during sintering above 1,300°C.

Carbon powder was reduced to the required size in a tungsten carbide percussion mortar.

3-1-2 Moulding

It was planned to mix up to as much as 50 volume %. of carbon into alumina powder to observe the effect of carbon for corrosion experiment. Therefore, carbon in proportions ranging from 30% up to 50% was added and pressed with the help of tragacanth solution to examine whether the compacts were strong enough to be handled during weighing, volume measurement and insertion into the furnace. As a result of this trial pressing, 30 volume % of carbon addition was found adequate to be handled without breakage.

Thus, 30 volume % of carbon and 70 volume % of alumina were mixed in a mechanical agate mortar for ten minutes to disperse the carbon powder uniformly into the alumina powder. Each volume of carbon and alumina powder taken was converted to the corresponding weight by multiplying by the appropriate true density. (3.96 gm/ml. for alumina and 2.05 gm/ml. for carbon). For example, weight for above proportion taken was

Weight of alumina   =   3.96 x 70/100

Weight of carbon   =   2.05 x 30/100

Then cylindrical pellets weighing about 1.5 gm each were pressed from both ends in a perspex lined steel mould, for minimizing impurities, by an hydraulic press with pressure of 9 tons/in^2.

3-1-3 Measurement of volume shrinkage

The volume of dried pellets before and after sintering was measured by the mercury balance. The detailed principle is described in chapter 4. Experimental techniques for corrosion.

3-1-4 Operation of experiments

The weighed and measured specimens, put into a carbon crucible, were pulled into the predetermined hot zone of a horizontal, tube furnace (see chapter 4) by means of a platinum - rhodium wire wound on a pulley (windlass), fixed at the end of the furnace tube. The photograph of the furnace is shown in figure 3-2. The specimens were kept for an hour in the hot zone. The sintering was done either in vacuo or in an atmosphere of flowing oxygen - free N_2. To ensure 100% nitrogen atmosphere, the inside of furnace tube was evacuated first.

The specimens after sintering were withdrawn to the cooler end of furnace tube by rotating the pulley. The chosen atmosphere was maintained until the specimens reached about $200^{\circ}C$. Before the next experiment, the Pt-Rh wire was stretched out to the other end of furnace tube.

3-1-5 Temperature measurement

An optical pyrometer, calibrated against 5% Rh-Pt versus 20% Rh-Pt thermocouple junction, was used, looking through a silica glass window placed on one end of the furnace. Discrepancies between the thermacouple junction and optical pyrometer reading was of the order of $20^{\circ}C$.

3-1-6 The observations made and results obtained

(a) Vacuum sintering

Carbon plus alumina pellets were sintered at 1,650°C for an hour to observe the sintering behaviour after some preliminary runs at lower temperatures. The volume shrinkage of these pieces was 2.7% which is considerably less than that of pure alumina at about 20% (18).

It was noticed during sintering that greyish coloured, highly porous substance with a bulk density of about 0.4 gm/ml. adhered around the open end of the furnace crucible. X-ray examination indentified the substance as aluminium oxide carbide (Al_4O_4C). The substance maybe formed under the reducing condition prevailing. It is evident CO gas is formed freely from carbon and alumina. This gas stream transports the Al_4O_4C (or its components) to the place where it was found. The X-ray pattern of this substance is shown in figure 3-3 together with the patterns of alumina and alumina plus carbon for comparison. The d-spacings of the adhered substance and aluminium oxide carbide are shown in Table 3-1.

Table 3-1   D-spacings of aluminium oxide carbide and the adhered substance (1).

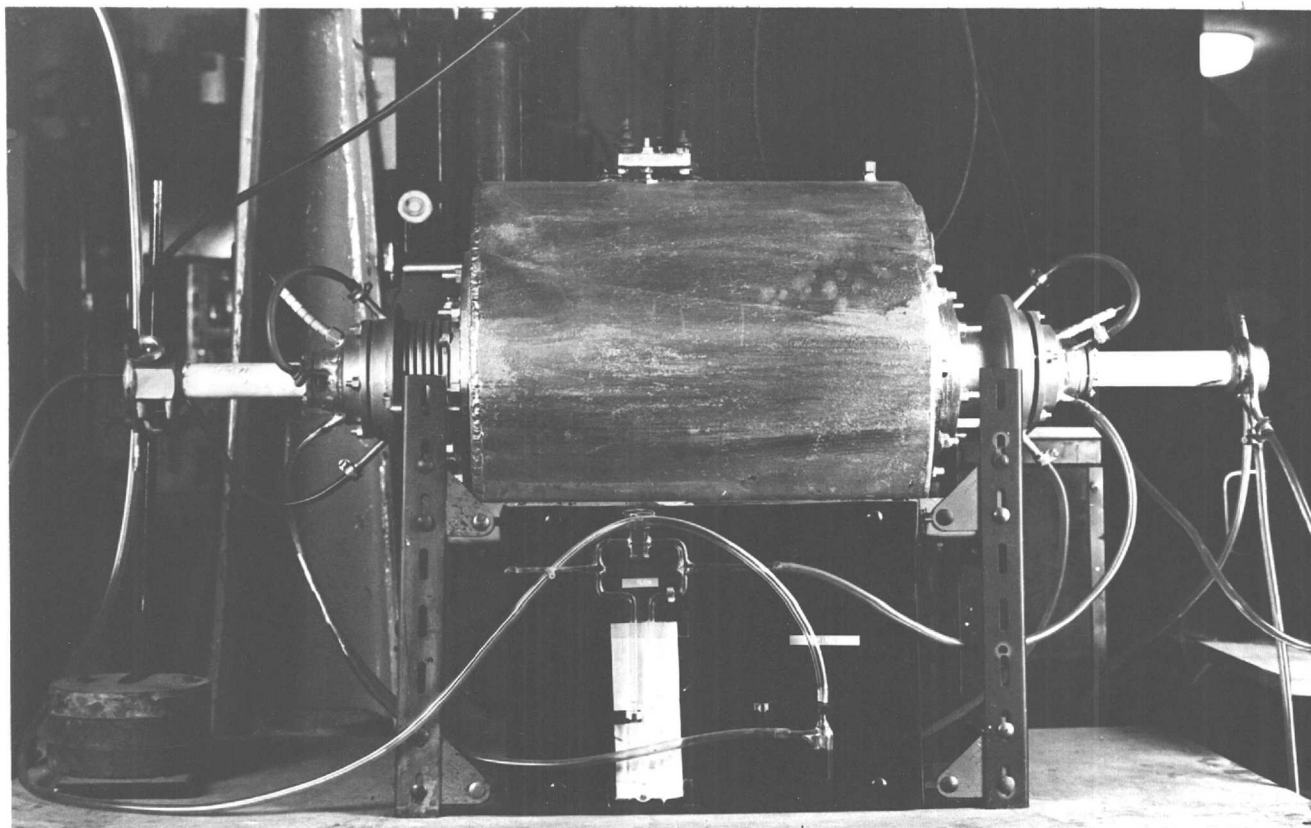| Aluminium oxide carbide	Adhered substance
d (A)	d (A)
4.22	4.20
3.87	3.86
3.30	3.30
3.11	3.10
2.48	2.43
2.32	2.32
1.49	1.49
1.45	1.45

Figure 3-2   Molybdenum-wound furnace.

(a)

(b)

(c)

Figure 3-3   X-ray powder patterns of (a) adhered substance, Al_4O_4C (b) alumina plus carbon (c) alumina.

(b) Sintering in oxygen-free nitrogen atmosphere

Since formation of the aluminium oxide carbide in vacuo spoiled the furnace tube, sintering was carried out in an oxygen-free nitrogen atmosphere with the hope of no formation of reaction product.

Volume shrinkage measurements and modulus of rupture tests have been done to observe sintering rate of carbon-containg alumina pellets and are shown in figure 3-4 and 3-5.

Surprisingly, $\Delta V/V$ curve shows volume of carbon-containing alumina has expanded approximately 0.15% from 1,300°C to 1,560°C as can be seen in figure 3-4. However, the modulus of rupture curve indicates that the strength of carbon/alumina composites has increased as shown in figure 3-5. The foregoing facts makes obvious that, in the presence of 30 volume % of carbon, the sintering of alumina was inhibited a great deal. The reasons for this could be considered as follows ;

(1) it may be supposed that the carbon would act somewhat like pores although carbon does not shrink or become eliminated like pores are during the sintering stage. Therefore, the addition of 30% of carbon would be expected hopefully to be similar to the addition of 30% of porosity to green pellet. But it proved to be wrong from the chemical point of view. As already mentioned a reaction product, aluminium oxide carbide, is formed in vacuo. It suggests alumina would be reduced to a sub-oxide of alumina, i.e. AlO or Al_2O, in the presence of carbon. As well aluminium vapour and CO gas would be formed. Mackenzie (25) relates how Al_2O is prepared by the heating of alumina in the presence of carbon at 1,300°C-1,500°C.
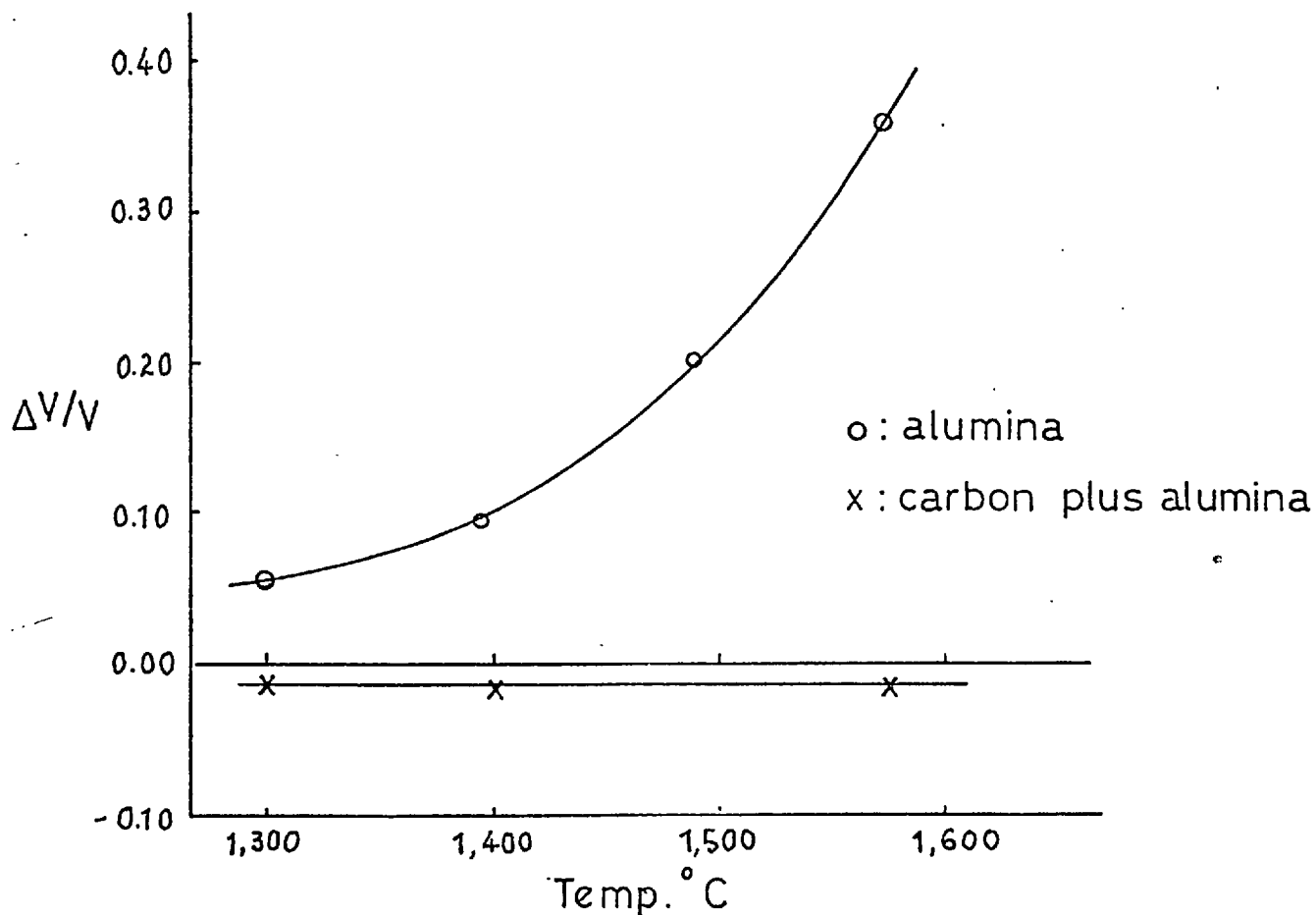
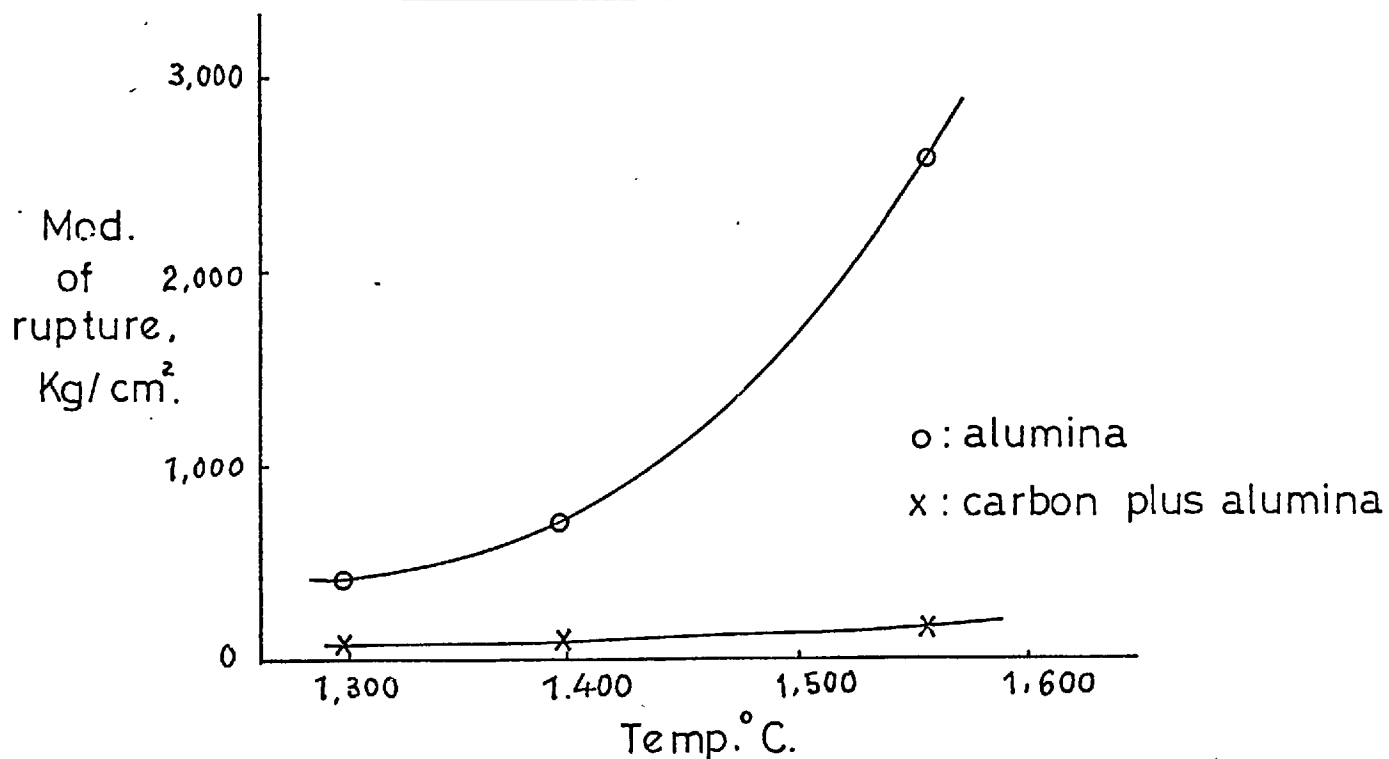Figure 3-4 $\Delta V/V$ againt temperature of (a) alumina and (b) carbon plus alumina in N_2 atms..

Figure3-5. Modulus of rupture against temp. of (a) alumina and (b) carbon plus alumina.

(2) during the first stage of sintering, neck growth between

adjacent particles occurs followed by volume shrinkage.

Also at this stage, carbon keeps the alumina particles

apart whilst as much as 30% of neck growth must be

occurring. Moverover as sintering of alumina proceeded,

it must be assumed that the carbon particles are placed

in compression by the shrinking alumina. This view was

supported by the observed fact that pellets sintered at

the highest temperature disintegrated into powder in air

a few days after the sintering during storage.

3-2 Impregnation of porous oxide refractories with carbon-containing substances followed by carbonization

3-2-1 Materials used

Sintered alumina

Sintered pure alumina rods, 2.6 cm. diameter x 23 cm.length,

fired at $1,600^{\circ}C$ and $1,700^{\circ}C$ supplied by Morgan Refractories were

used throughout this part of the investigation. The chemical

analysis given by the manufacturer is shown below ;

Composition	%
Al_2O_3	99.70
SiO_2	0.05
Fe_2O_3	0.10
Na_2O	0.20
K_2O	0.05

The true porosity and bulk density (which was the average

of numerous measurements) are given below ;

Sintering temperature $^{\circ}C$	Bulk density gm/cm^3	True porosity %
1,600	2.80	29.2
1,700	3.11	21.3

Impregnants

What is required for impregnants in the present research was the substance with high carbon content, having good pore penetration properties. Ideally it is better to be a liquid which changes into a solid phase by heat treatment and can be heated to a high temperature to deposit a high proportion of carbon in the pores of refractory oxides without passing through the liquid phase.

To suit the above requirements, furfuryl alcohol and "Cascote" resin were found to be adequate, which was chosen to produce impervious graphite by Watt and Johnson (40) and Graham, Campbell and perels (15). But in the brick industry, pitch was preferred as a source of carbon in impregnated MgO - CaO refractories and also as temporary binders in pitch - bonded and tempered MgO - CaO refractories, for its low cost and abundance. Bearing in mind what is used in industry, pitch was mainly chosen for a carbon former in present research as well as "Cascote" resin to assess the effect of carbon formed form different sources.

The pitch used was lean tar pitch produced as a by-product of the distillation of coal. It was supplied by The Coal Tar Research Association. Their elementary analysis of the pitch was approximately C = 92.4%, H = 4.5%, N = 1.0% the balance being mainly oxygen and some sulphur. The softening point of this pitch was $85^{\circ}C$ (34).

"Cascote No. M558" resin was obtained from Mr. W. Johnson of the Royal Aircraft Association. This is a commercial furane product made by the Borden Chemical Company. It is a partially polymerized mixture of furfuryl alcohol and furfuraldehyde.

This impregnant was used diluted with 100 parts of acetone to
lower the viscosity for the improvement of penetration, to which
5 parts of acid catalyst was added for polymerization. The mixture
had a usable life in air in excess of 24 hours.

3-2-2 Methods of impregnation

The principle of the technique adopted was basically the
same as the standard test method for the determination of porosity
and density. (the evacuation method.) In this method, the pores
of ceramics are filled efficiently with water.

Pitch impregnation

The dried and weighed, half-moon shape sintered alumina
pieces (preparation of specimen is described in Chapter 4) were
immersed in pitch near its boiling point. Vacuum was applied for
30 minutes and air then admitted to allow molten pitch to penetrate
through the open pores of the alumina. Then the specimen were
lifted out by means of a pair of tongs and molten hot pitch
adhering to the surface of specimen cleaned off with a tissue.
Fresh pitch was used for each impregnation to keep the viscosity the same.

"Cascote" resin impregnation

The weighed specimens, put into the beaker, were placed
in an empty desiccator. The pressure in the desiccator was
reduced down to 1 cm. of mercury, and the "Cascote" resin mixed
with catalyst was then admitted slowly. The reduced pressure was
maintained until the specimen were covered with liquid resin.
The immersed test pieces were kept under reduced pressure for half
an hour. The air was then introduced after this process and the
specimen were lifted out by the aid of a pair of tongs. The surfaces
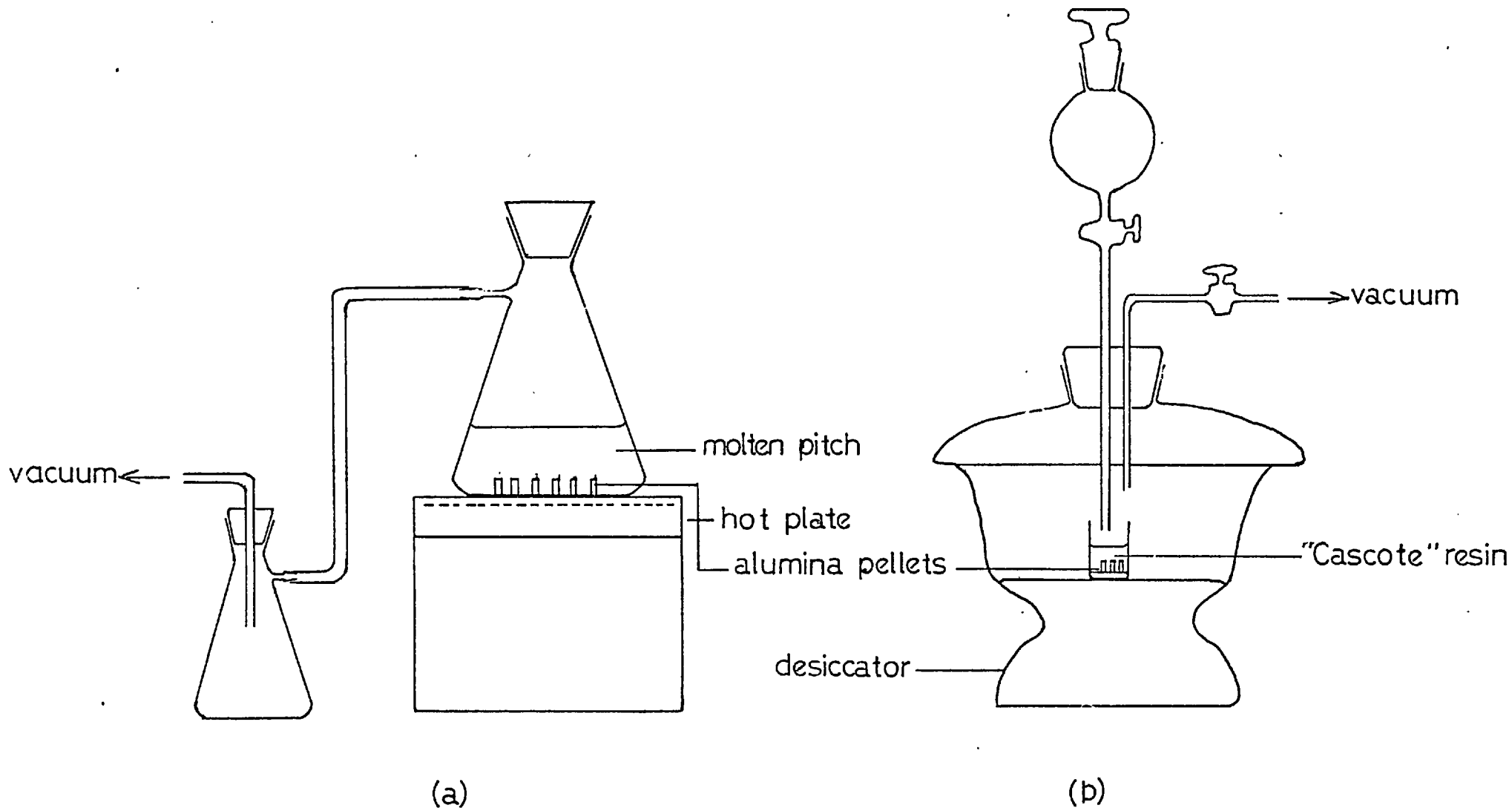of the specimens were cleaned by brief contact of a tissue.

vacuum ←

molten pitch

hot plate

alumina pellets

vacuum →

"Cascote" resin

desiccator

(a)

(b)

Figure 3-6. Diagram of the apparatus used for impregnation of refractories by (a) pitch and (b) "Cascote" resin.

These specimens were polymerized in an electric oven at 120°C overnight. The apparatus for both pitch and "Cascote" resin impregnation is shown in figure 3-6.

3-2-3 Carbonization

The object of carbonization was either to decompose the pitch or to break down the polymer, leaving the thermally stable carbon in the pores of alumina, which would not undergo any structural change itself during the corrosion experiment. As most of the corrosion experiments were planned to be performed around $1,000^\circ$C, the temperature for carbonization was therefore chosen at $1,200^\circ$C.

The impregnated specimens put into the alumina crucibles were pushed slowly into the uniform hot zone of the molybdenum-wound tube furnace. The furnace for carbonization was the same as the one used for the sintering shown in figure 3-2. The specimens were kept at $1,200^\circ$C for 30 minutes in an atmosphere of flowing oxygen-free nitrogen. The windlass system, divised for the sintering of carbon/alumina composites, was found impossible to use because the Pt-Rh wire was easily broken due to the sticking of the crucible to the furnace tube caused by melting of adhering pitch around the specimens. The specimens after carbonization were withdrawn to the cooler part of the furnace tube and finally taken out when the specimens reached 200°C. Carbon adhering around the specimens, noticed with pitch-containing pellets, was removed by rubbing with a knifedge. To increase the quantity of carbon in alumina, carbonized pellets were impregnated and carbonized again.

The weight increase of the specimens was measured and the percentage of carbon in alumina was calculated by dividing the

weight increase by the weight of alumina.   Typical percentage
increases in carbon due to pitch and "Cascote" resin impregnation
is shown in Table 3-2.

Table 3-2

	Pitch		"Cascote" resin	
	Porosity	Carbon gained	Porosity	Carbon gained
Specimen No.	%	% by wt.	%	% by wt.
1	29.06	3.71	29.92	2.67
2	30.51	3.72	29.94	2.82
3	29.95	3.70	28.68	2.75
4	29.91	3.77	28.75	2.70
5	30.56	3.71	30.11	2.69

Chapter 4

Experimental techniques for corrosion.

4-1   Materials

4-1-1   Oxide refractories

4-1-2   Melts

4-1-3   Crucibles

4-2   Preparation of the specimens

4-2-1   General preparation

4-2-2   Volume measurements – Mercury balance

4-2-3   Surface area measurement of the specimens

4-3   Furnaces and temperature control

4-3-1   Kanthal – wound furnace

4-3-2   Platinum – wound furnace

4-3-3   Molybdenum – wound furnace

4-4   Experimental procedure for the corrosion experiments

4-4-1   Continuous weighing technique

4-4-2   Static corrosion experiments

Chapter 4

Experimental techniques for corrosion

General plan

Because alumina, silica and magnesia are the main

constituents of refractories commonly used in industry, these

materials were chosen to determine the corrosion rates in

melts. Preliminary experiments were carried out with single

crystal and porous, pollycrystalline materials. Melts chosen

were sodium tetraborate, sodium metavanadate, sodium carbonate

and sodium silicate which melt at moderate temperatures well

below 1,000°C and were used previously in the laboratory.

But it was found that silica and magnesia did not meet the

requirements for quantitative measurements in above respect.

In detail, sintered porous silica cracked when it was exposed

to heat for the corrosion experiments because of the cristobalite

crystals developed during the sintering at 1,350°C. The

percentage of cristobalite was determined by measuring the area

under the high-low cristobalite inversions. Since no results

are reported on the corrosion of silica specimen, nothing further

will be said on this point. Magnesia was disintegrated while the

adhering melt on corroded specimens was removed in dilute HCl

solution. This particular problem could have been overcome by

employing the continuous weighing technique which does not involve

a cleaning procedure, previously used by Safdar and Barham (33)

(2). However, gas bubbles evolved, when the carbon-containing

pellet was dipped in melt would most likely yield serious experimental

errors. Therefore, experimental work was confined to alumina by

the static corrosion experimental technique.

4-1 Materials

4-1-1 Oxide refractories

Commercially supplied single crystal alumina half boules, 7cm. long and 2cm. in. diameter, were obtained from the Crystal Growing Laboratory at the Department of Electrical Engineering of Imperial College. Porous alumina pellets prepared in the laboratory and commercially sintered alumina, described in section 3-2, were used. The sintering technique and qua-lity of alumina used were the same as the sintering techniques for carbon-containing alumina pellets, described in section 3-1.

Two forms of magnesia were used, namely (1) single crystal (2) porous magnesia discs produced by the sintering in the laboratory at 1,450°C for an hour. Fused magnesia powder was supplied by Super Refractories LTD., with quanranteed purity of 99.9%.

Rod of transparent silica glass, 1 inch in diameter was supplied by the Thermal Syndicate.

4-1-2 Melts

Fused sodium tetraborate, sodium metavanadate and sodium carbonate were obtained from Hopkin and Williams. Sodium silicate was given by Joseph Crossfield and Son. It contained 22.9 weight % of Na_2O and 76.7 weight % of SiO_2 and melted at 780°C.

4-1-3 Crucibles

Pt-20% Rh crucible, 10cm. long and 5 cm. in diameter, was used contain the melts of 200 gms. It was always supported by a closely fitting fully sintered alumina crucible.

4-2 Preparation of specimens

4-2-1 General preparation

The sintered discs, about 2mm. - 3mm. thick and 2.0cm. in diameter, were sawn down the middle to form two half-moon shapes.

Those materials which were in the form of cylindrical rod were cut by a diamond saw into pieces about 2mm. thick and these discs were sawn in the middle. The rough surfaces of all test pieces were ground by a diamond cup wheel and cleaned in dilute HCl solution followed by distilled water before drying to constant weight in an electric oven at $120°C$.

To deposit carbon in the pores of alumina, porous alumina pieces were impregnated with either pitch or "Cascote" resin by the procedure already described in section 3-2. The carbon adhering on the surfaces of carbonized specimens was removed by grinding on a diamond wheel. The specimens were then cleaned and dried to constant weight.

4-2-2 Volume measurements - Mercury balance

Mercury balance

Volume of the pellets were measured by the mercury balance. The idea of the mercury balance was originally devised to measure the volume of brick in early 20th century by Westman (41), followed by Clark and White (7) and further developed and used by Hill (18) and Philopoulus (28).

The basic principle is to measure the upthrust, due to the weight of mercury displaced by the specimen, as the specimen is submerged in a claw, attached beneath the balance pan. The weight of specimen added to upthrust weight devided by the density of mercury will give the volume of pellet as shown below ;

$$\text{Volume} = \frac{W' + W}{D_{Hg}}$$

W' : the upthrust weight

W : the weight of specimen

The bulk density of the pellets were calculated and the

percentage of true porosity was also calculated by the following

formula ;

$$\text{True prosity (\%)} = 100 \ \left(1 - \frac{\text{bulk density}}{\text{true density}} \right)$$

During the course of measurements, clean mercury was

found to be essential to measure the volume accurately. Because

in the presence of ceramic dust, it tends to cling to the stem.

Thus, mercury was regularly cleaned by passing it through dilute

nitric acid solution repeatedly in the form of small droplets.

In case the ceramic powder was noticed on the surface of mercury

in between the measurements, having dropped from the friable

edges of the dried compacts, it was removed by passing mercury

through a small hole made in the bottom of the filter paper

wrapped into a conical shape.

Care was taken not to introduce air bubbles into mercury

while the specimens were being immersed. This was managed by

first submerging the specimen, beneath the mercury with a finger

tip and then enclosing the specimen by the claw, pushed under

the mercury.

4-2-3 Surface area measurement of specimens

The geometrical surface area of the specimens was measured

by the method used previously in our laboratory. The curved area

of flat parts of the specimens was measured by counting the area

of the specimen pressed on graph paper. The average thickness of the specimen was measured at five different places with a micrometer screw gauge. The edge area of the specimens was obtained by multiplying the average thickness by the edge length measured by the vernier.

4-3 Furnaces and temperature control

4-3-1 Kanthal - wound furnace

The coiled coil of Kanthal wire was wound on a 3-inch outside diameter, recrystallized alumina tube. The furnace was insulated by expanded vermiculite contained in a metal casing. Power was supplied from the mains to the furnace through a continuously variable transformer. The furnace temperature was controlled up to $1,200^{\circ}C$ by a platinum 13% rhodium thermocouple connected to an on - off type automatic controller made by Shinko Electric Instruments, Japan.

4-3-2 Platinum - wound furnace

This was a commercial platinum, wire - wound tube furnace, 1.5-inch in diameter, supplied by Johnson and Matthey for use up to $1,500^{\circ}C$. The furnace temperature was controlled by a platinum 13% rhodium thermocouple connected to a Kent automatic controller.

4-3-3 Molybdenum - wound furnace

During the course of the research especially when temperture above $1,500^{\circ}C$ were required, a tube furnace was assembled by following the procedure described in the article by Barrett (3), molybdenum tape was wound on a 3-inch diameter impervious alumina tube. Both ends of the furnace tube adjoining the furnace casing, were sealed at first by the customary method adopted since the earliest days in the ceramics laboratory. The gas tightness was

20 19   18   17 16 15 5   14   13 12 11 10 9 8 7   5   6 5 4 3 2 1
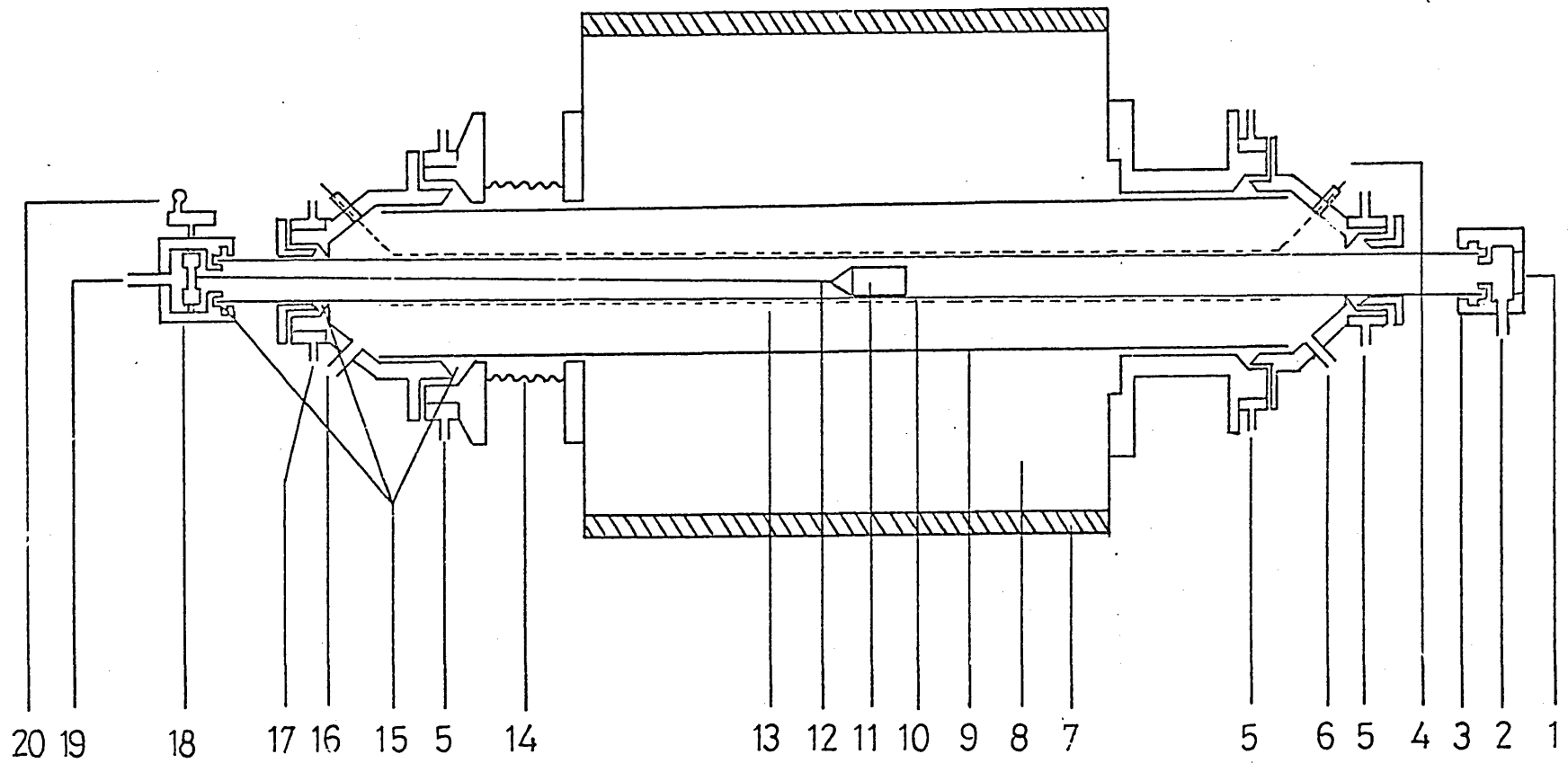
Figure 4-1   Molybdenum-wound furnace.

ensured by tapered metal rings pressed on an asbestos packing by

clamping down through suitable fittings. Molybdenum tape was

prevented from oxidation by providing an atmosphere of flowing

mixed gas ; 10% hydrogen and 90% nitrogen (hydrogen forming gas).

But this arrangement was found inefficient, because the inside of

the whole furnace casing has kept leak tight. Therefore, the

arrangement was modified later on, as shown in figure 4-1.

The modified furnace consisted of 1.4-inch diameter imper-

vious alumina inner tube (10) - the numbers refer to the corres-

ponding numbered components in figure 4-1 - on which molybdenum

tape (13) was wound and 3-inch diameter alumina tubes (9) (10)

were sealed by the water cooled (5) (17) rubber "O" rings (15).

Hydrogen forming gas was passed through (6) (16) in between these

two furnace tubes. The furnace was insulated with coarse fused -

alumina grain (8) and 2 cm. thick layer of fibrous alumino -

silicate wool (Kao-wool) (7) inside and immediately next to the

furnace casing. Power was supplied through a voltage stabilizer

("Regavolt") and the furnace temperature was controlled by a trans-

former and an on-off type Kent automatic controller. This furnace

was capable of going up to $1,800^{\circ}C$ and temperature was measured and

controlled by a 5% Rh-Pt versus 20% Rh-Pt thermocouple.

4-4 Experimental procedure for the corrosion experiments

Melt contained in a platinum crucible supported by the sin-

tered alumina crucible was lowered into the predetermined hot zone

of the vertical, Kanthal - wound tube furnace by means of a pair

of tongs. The crucibles were seated on a sintered alumina cylinder

fitted on an adjustable pedestal place at the bottom of

tube furnace, The controlling thermocouple junction embedded

in the alumina cylinder was situated beneath the crucibles.

The actual temperature of the melt was measured by a bare ther-

mocouple put into the melt.

4-4-1 Continuous weighing technique

Preliminary work was carried out by the continuous weigh-

ing technique which is shown in figure 4-2.

The specimen, suppended on a platinum wire through a hole

made by a diamond drill, was lowered in stages towards the melt.

The specimen was left just above the melt for a few minutes to

reach thermal equilibrium with the melt. After the specimen was

immersed in the melt, 20 - 30 seconds elapsed before the first

reading although a good prior estimate of the correct weights

was already put on the balance pan. Thus, the first reading

was taken a minute after immersion and the following readings

were taken at planned time intervals by removing the weights from

the balance. These weight decrements were converted to actual

weight loss of refractory in the melt (see Chapter 6). After

each run, which last generally an hour, the specimen was removed

quickly from the melt and then cleaned in hot dilute HCl solution

followed by distilled water and finally dried to constant weight.

This overall weight loss was used to compare the weight loss

obtained from the calculation.

The density of melt was obtained by using Archimedes'

principle. Buoyancy of a platinum sphere in the melt was measured

by the same procedure as described above. The weight of platinum

sphere divided by the volume of platinum at that temperature gave
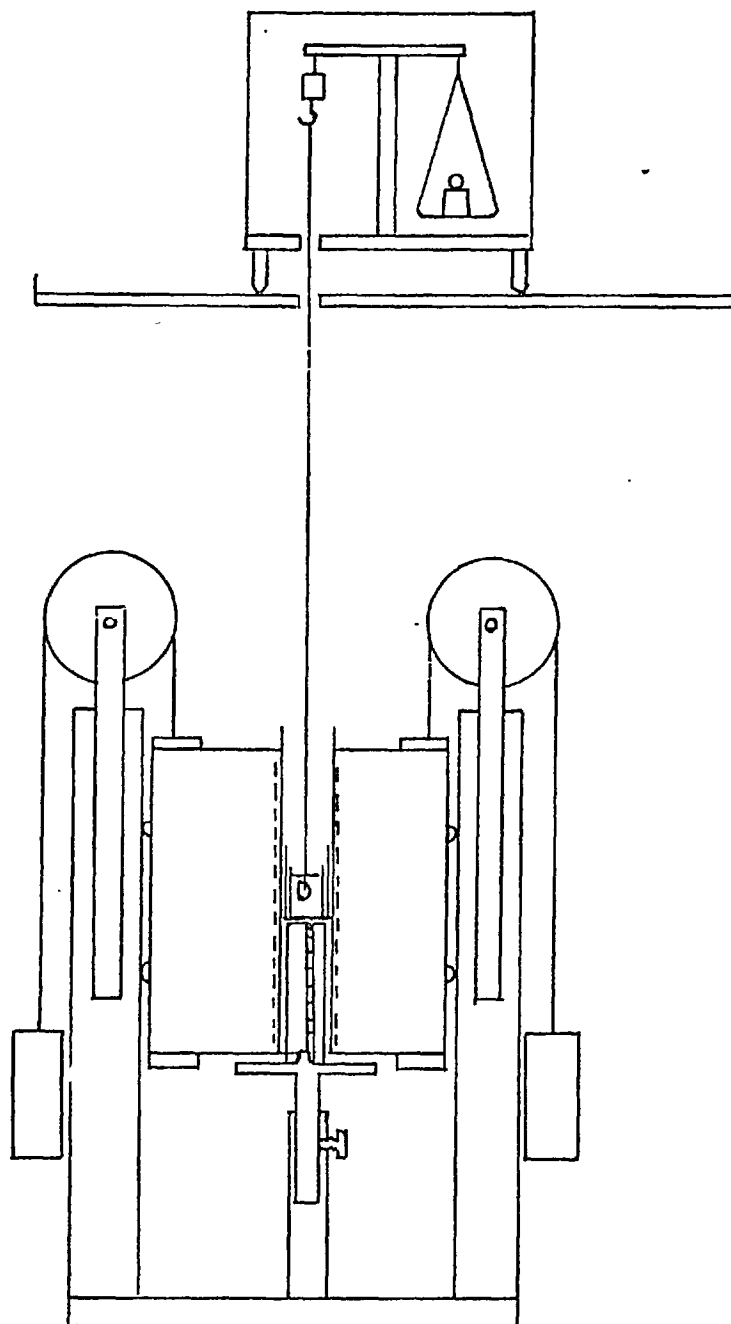
the density of the melt.

Figure 4-2   Continuous weighing apparatus.

4-4-2 Static corrosion experiments

To prevent weight loss of carbon-containing alumina by oxidation while the composite specimen was immersed and removed from the melt, it was decided to perform these operations in a nitrogen atmosphere. Thus both ends of the vertical Kanthal - wound furnace tube were closed by suitable fittings. A photograph of the apparatus is shown in figure 4-3.

The top of the furnace tube was closed by a water - cooled metal fitting suitably made to hold the alumina tube, to which was attached the platinum holder. A photograph of the platinum holder is shown in figure 4-4. This alumina tube was capable of sliding up and down by an asbestos packing used in the top enclosure of the furnace tube. The bottom of the furnace tube was sealed with the help of pressed "Kao - wool".

The specimen, retained in the two clamping rings of the platinum holder, previously used by Faruqi (11) for a similar purpose, was inserted in the nitrogen atmosphere of the furnace and held by the top fittings as described above. The specimen was lowered near to the melt and left just above the melt for a few minutes to reach the same temperature as melt. The specimen was immersed in the middle of the melt for a predetermined time.

The corroded specimen was removed from the melt and left in the cooler part of the furnace to cool down for a few minutes before it was taken out of the furnace. The adhering melt around the corroded specimen was removed in hot dilute HCl solution, followed by distilled water and then the specimen was dried to a constant weight.

The weight loss obtained by this thermogravic method was
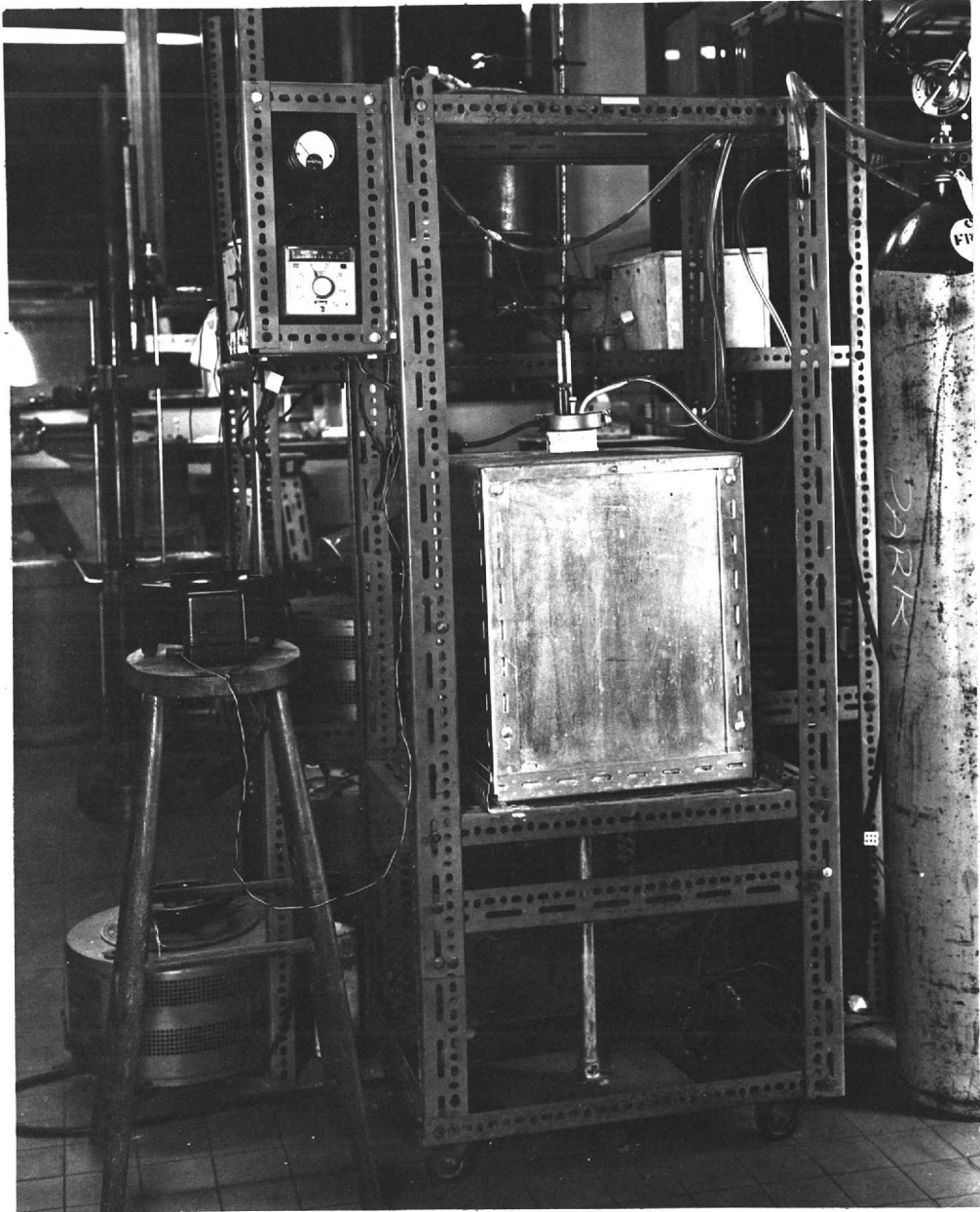
Figure 4-3 Apparatus for static corrosion experiments.(left)
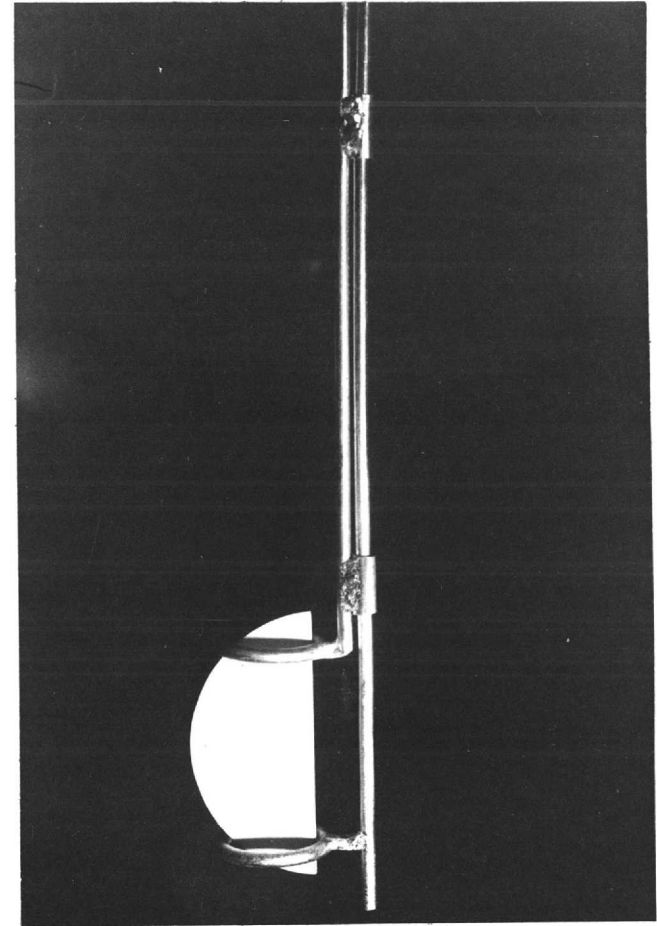
Figure 4-4 Platinum holder.(above)

used to calculate the weight loss/unit area of the specimen.
A fresh specimen was used each time to obtain a point on the
weight loss/unit area against time curve.

Chapter 5

Some observations made on the oxidation of carbon in air and in melts at elevated temperatures.

Chapter 5

Some observations made on the oxidation of carbon in air and
in melts at elevated temperatures.

5-1 Aims of the work

As the main object of the present research was to under-
stand the role of carbon in carbon-containing refractories under
melts with respect to the corrosion resistance of refractories,
it was considered an essential pre-requisite to investigate the
behaviour of carbon itself in the melts. It was also hoped
that the mechanism of corrosion of carbon-containing refractories
in the melts would be easier to assess by simplyifing this
complex situation, i.e. carbon-refractory - melt to carbon -melt
and refractory - melt.

Oxidation of silicon carbide under a melt studied by
Smith (36) suggested carbon would also be oxidized in the melts
in the presence of air either by atmospheric oxygen or oxygen in
the melt. Hence the amount of carbon oxidized in the melts, in
the presence of air at several different temperatures, was deter-
minted by weight change. Also the oxidation rate of carbon, in a
steady flow of air, was measured since it was felt desirable to
estimate the combustion rate of the particular carbon (CY9) used,
over the temperature range in which the experiments on the oxida-
tion of carbon in the melts were conducted.

5-2 Experimental procedure

5-2-1 Combustion of carbon in a steady flow of air

A schematic diagram of the apparatus for the determination
of the combustion rate of the carbon in air is shown in figure 5-1.
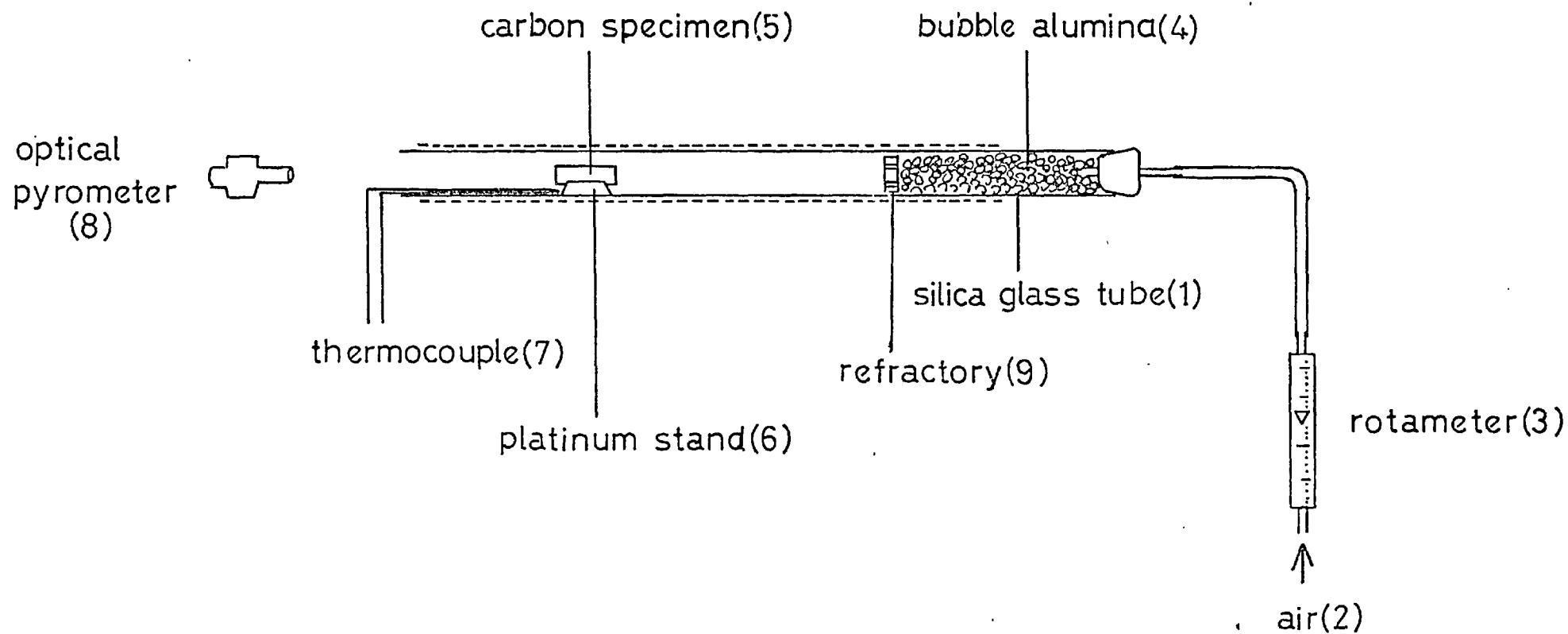
Figure 5-1 Diagram of the apparatus used for the oxidation of carbon in air.

A horizontal silica - glass tube furnace (1), about 3 cm. in outside diameter, was used. Compressed air (2) from the laboratory air line which was metered by the rotameter (3), was passed through the preheating part of the furnace packed with the bubble alumina (4).

A carbon specimen, about 2 cm. long and 1.3 cm. in diameter, was cut from cylindrical rod of carbon supplied by the Morganite LTD. (CY9). This (5) was seated on the knifedge of the platinum stand (6) and inserted into the predetermined uniform hot zone of the furnace tube. A platinum, 13% rodium platinum thermocoupe (7) was used to measure furnace temperature. But the temperature of the carbon surface was measured by an optical pyrometer (8) calibrated against standard thermocouple.

The duration of experiments was one hour and the starting time of combustion was taken when the carbon specimen began to appear to be burning at a steady rate, in the period of 2-5 minutes depending upon the temperature employed after the carbon rod was inserted into the furnace. The combustion temperature was obtained by averaging the temperature of the carbon surface measured at 5-10 minutes intervals.

The geometrical surface area of the specimen tended to decrease more at a higher temperature and quite appreciably. Hence an average of a initial and final surface area was taken for the weight loss/unit area calculation. The initial surface area was calculated from the measurement by a micrometer screw gauge. The final surface area was obtained from the curve in which is plotted surface area against the weight of the carbon.

5-2-2 Oxidation of carbon under the melts

The apparatus and experimental technique employed were the same as those of the static corrosion experiment for the carbon-containing alumina described in section 4-4-2, .except for a change of atmosphere from nitrogen to air. To avoid an overlapping explanation of the experimental procedure, the few different arrangements made will thus be described in this section.

The carbon specimen, preheated up to about 300-400°C, was immersed immediately into the melt without allowing it to reach thermal equilibrium with the melt, to avoid weight losses by oxidation in the air ; similarly the oxidized specimen was removed directly from the melt to the cooler part of the furnace tube, below 400°C.

The carbon used was in the form of cylindrical rod, slightly less than 3 cm. in diameter, supplied by Morganite LTD.(CY9). The properties as given by the manufacturer, are shown in Table 5-1 together with graphitized carbon (EY9). The rod was cut into pieces about 3 mm. - 4mm. thick by a saw and these discs were cut in the middle to form two half-moon shapes to be fitted in two rings of the platinum holder. The uneven surfaces of carbon were ground by rubbing on emery paper. The geometrical surface area of the specimens was measured in the same manner as described in section 4-2-3.

To determine the amount of carbon oxidized in sodium silicate a vertically placed platinum - wound tube furnace was used as temperature of the experiments was around 1,200°C or even higher. In this instance 50 gms. of the melt contained in a platinum crucible about 6 cm. long and 3 cm. in diameter, was used.

Table 5-1   Properties of carbon

Property	Carbon (CY9)		Graphitized carbon (EY9)	
	Longitutional	Transverse	Longitutional	Transverse
Bulk density, gm/cc.	1.57	1.57	1.68	1.68
Open porosity, %	18.4	18.7	17.6	17.5
Compressive strength, Kg/cm^2	700	545	500	480
Breaking strength, Kg/cm^2	190	175	275	200
Resistivity, 10^{-4}Ohm.cm.	22.9	42.7	18.8	39.4
Thermal expansion, $10^{-6}/^{\circ}C$	1.43	4.26	1.8	4.0
Thermal conductivity, W/cm$^{\circ}$C	0.35	0.21	0.58	0.46

Table 5-2   Combustion rates of carbon in a steady flow of air.

(air velocity :   3.73 cm/sec.)

Temperature, $^{\circ}$C	Weight loss gm/cm^2/hr.	Temperature,$^{\circ}$C	Weight loss gm/cm^2/hr.
580	0.0239	720	0.2623
600	0.0392	779	0.3062
630	0.0765	870	0.3662
656	0.1556	952	0.3958
680	0.1910	1,113	0.4543

Oxidation rate of carbon in the melts.

Temperature, $^{\circ}$C	$Na_2B_4O_7$	$NaVO_3$ (gm/cm ^{2}/hr.)	$Na_2O.2SiO_2$
700	–	0.0114	–
800	0.0008	0.0272	–
900	0.0020	0.0926	–
1,000	0.0037	0.1653	–
1,050	–	–	0.0019
1,070	0.0069	–	–
1,100	–	0.2134	0.0045
1,150	0.0132	–	0.0095
1,200	–	–	0.0138

Table 5-3   Activation energy for the oxidation of carbon in

air and in the melts.

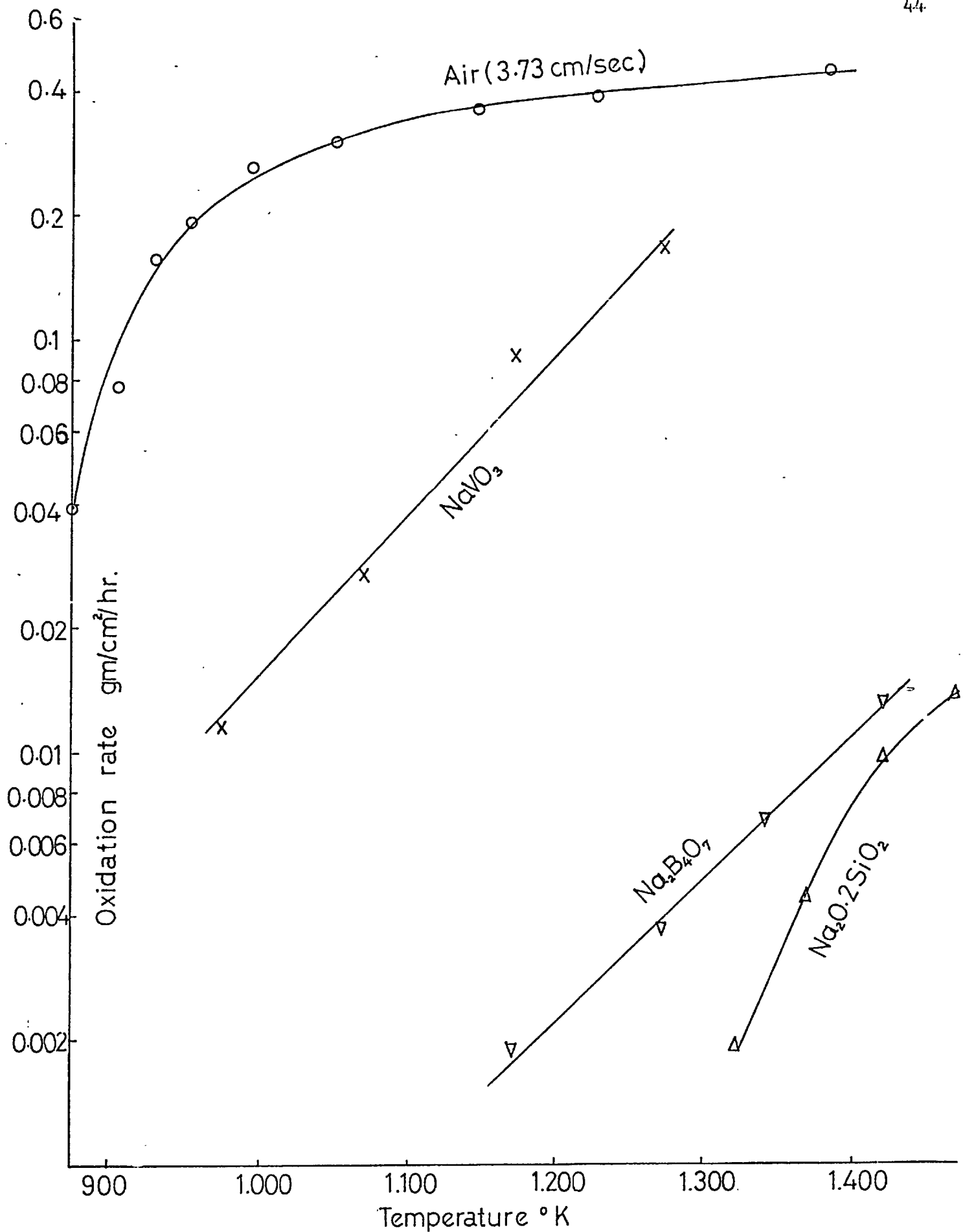|	Activation energy, Kcal/mol.
Oxidation of carbon in $NaVO_3$	22 (973 – 1,273°K)
Oxidation of carbon in $Na_2B_4O_7$	23 (1.073 – 1,343°K)
Oxidation of carbon in $Na_2O.2SiO_2$	61 (1,323 – 1.423°K)
	24 (1,423 – 1.573°K)
Oxidation of carbon in air (author)	31 (below – 1,000°K)
	4 (above – 1,000°K)
(Tu, Davis and Hottel)	35 (below – 1,100°K)
	2 (above – 1,100°K)

Figure5-2 The rate of oxidation of carbon in air and in the melts above 900°K.
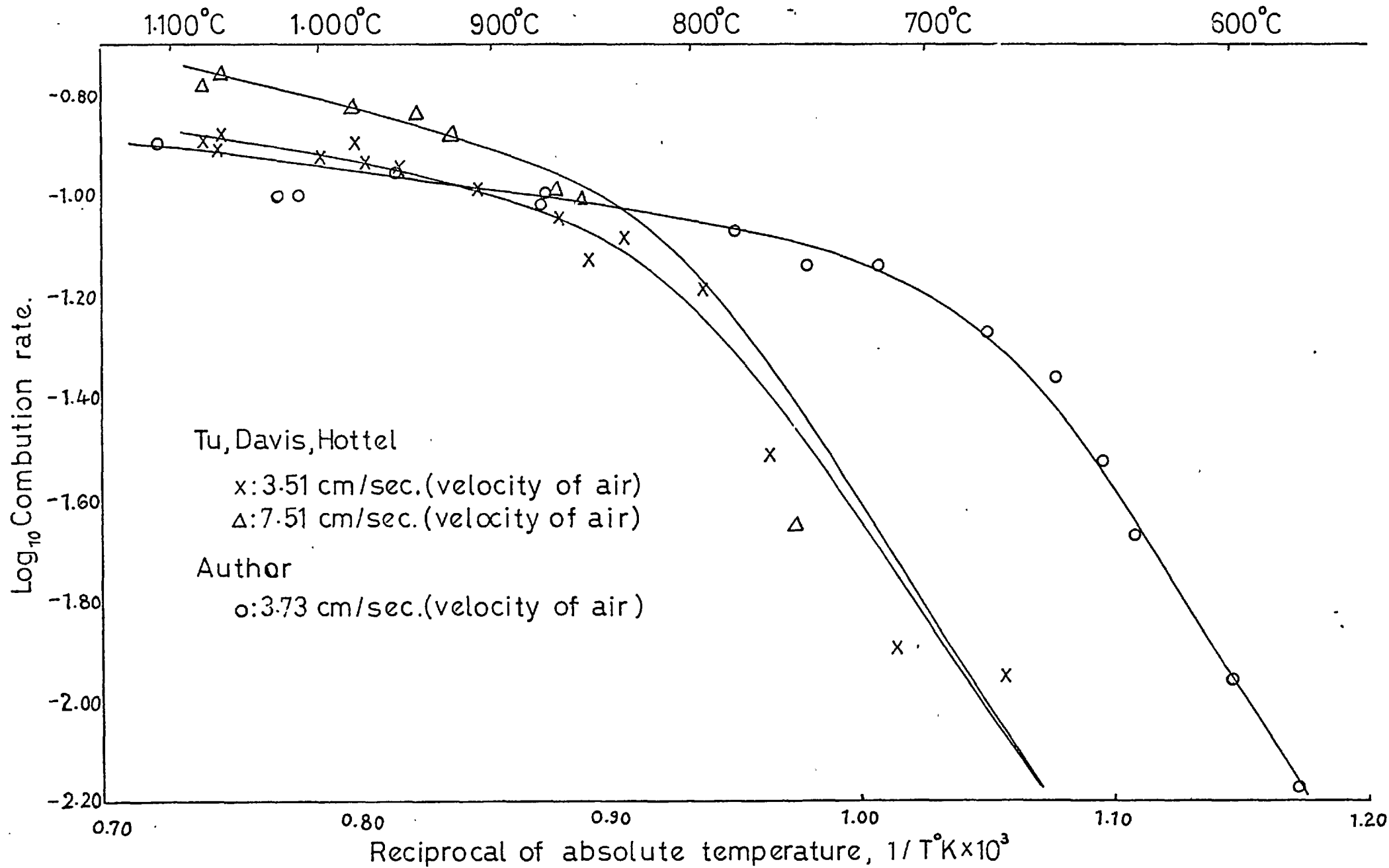
Figure 5-3 Arrhenius plot of the rate of oxidation of carbon in a steady flow of air.
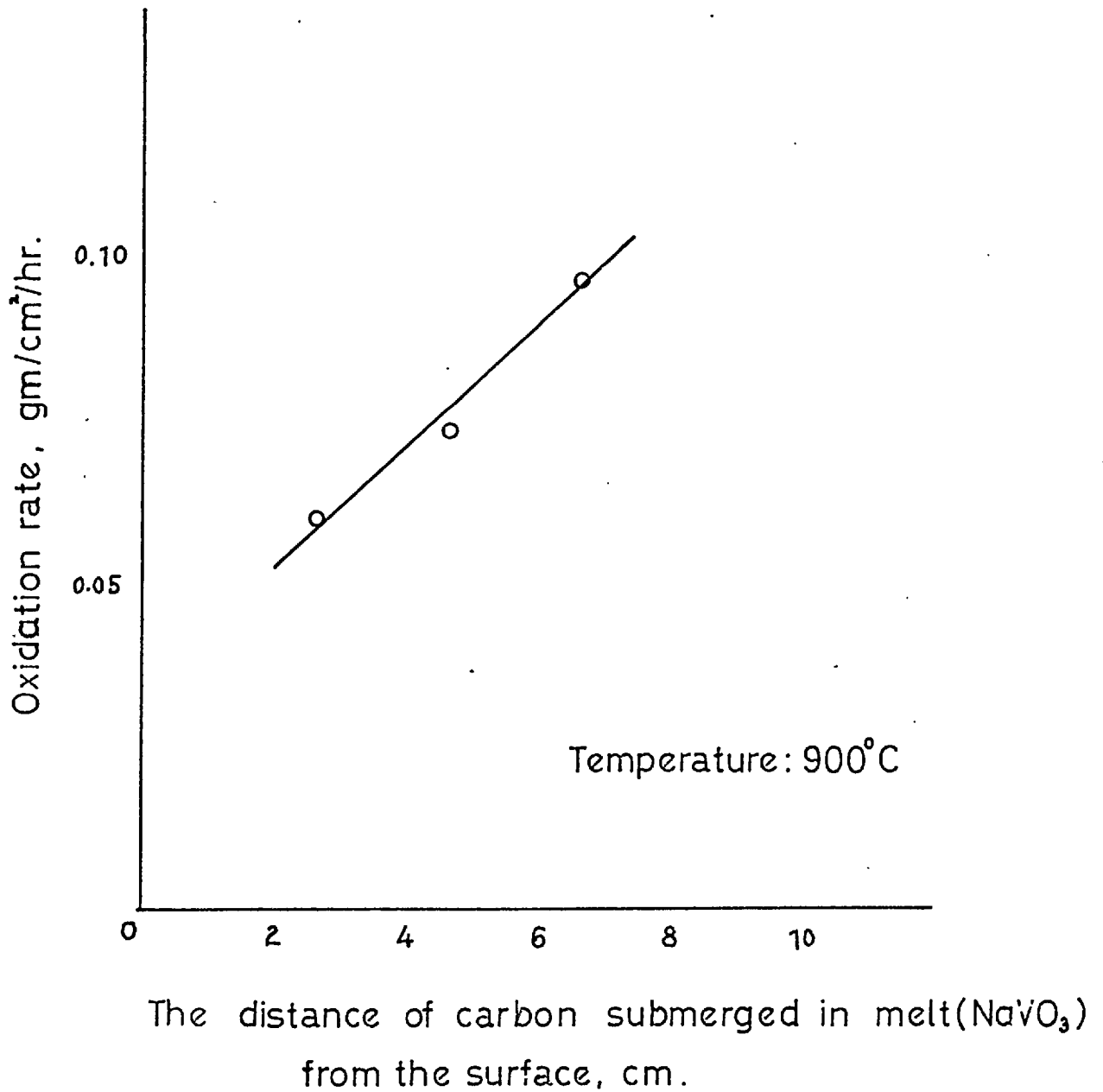
45

Figure 5-4 Arrhenius plot of the rate of oxidation of carbon in melts(air over melts)

x: Sodium metavanadate
o: Sodium tetraborate
Δ: Sodium silicate
+: Sodium metavanadate
(N_2 over the melt)

Reciprocal of absolute temperature, $1/T°K \times 10^3$

The distance of carbon submerged in melt($NaVO_3$) from the surface, cm.
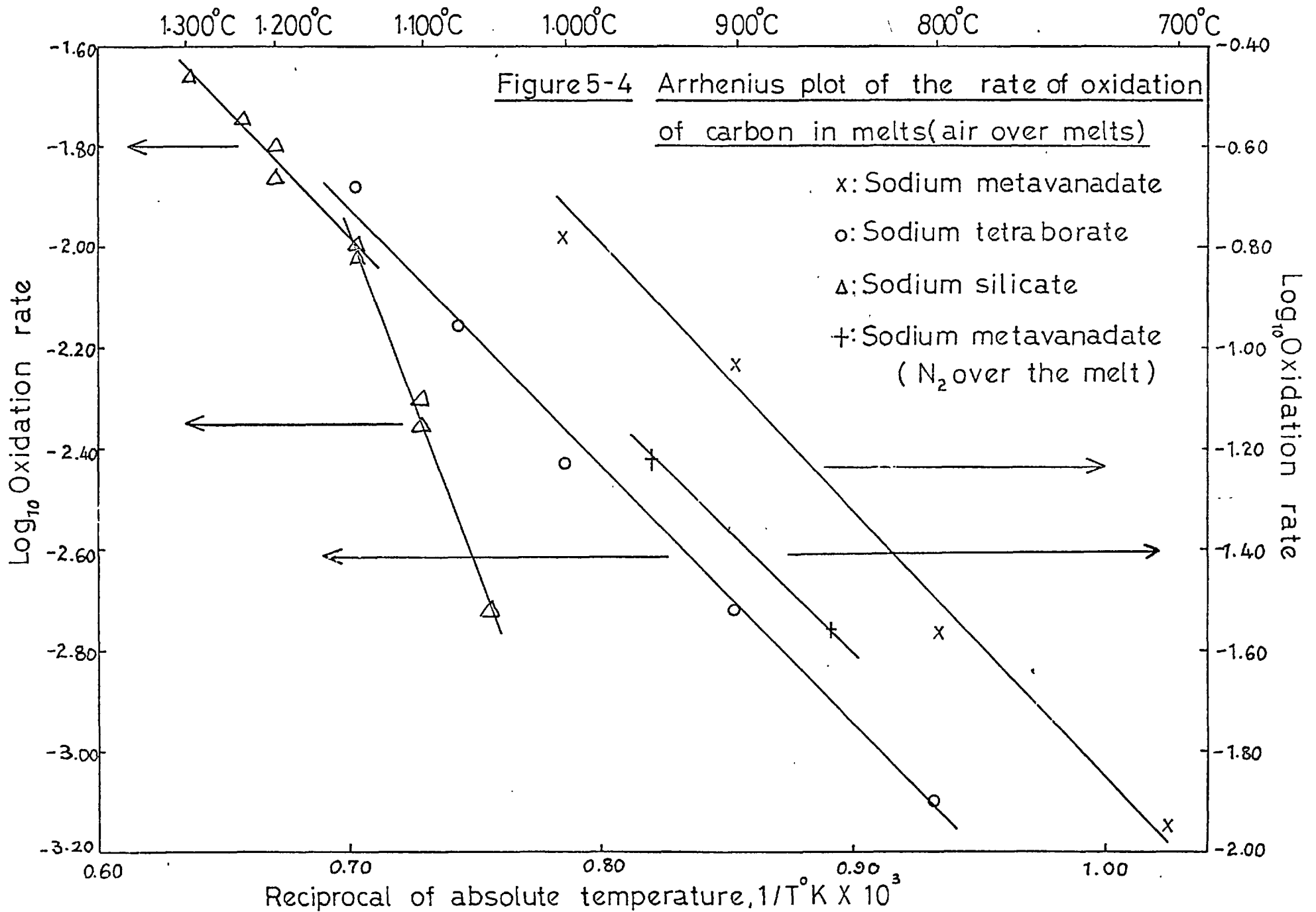
Figure 5-5. The oxidation rate of carbon vs. the distance of carbon submerged in melt ($NaVO_3$).

5-3 Results

The amount of oxidation of carbon in air and in sodium
metavanadate, sodium tetraborate and sodium silicate melt was
measured over the range of temperature from $700^{\circ}C$ to $1,200^{\circ}C$.
The oxidation rate $(gm/cm^2/hr.)$ is tabulated in Table 5-2 and
plotted in figure 5-2, on a logarithmic scale of oxidation rate
against absolute temperature of the carbon surface, together
with that of carbon in the melts, in which instance the absolute
temperature of the melts was taken.   The activation energies
for the oxidation were calculated from the Arrhenius equation ;

$$K \quad = \quad A \exp \; (^{-E}/RT)$$

$$Log_{10} K \quad = \quad Log_{10}A - E/4.575T$$

or

the slope of the $Log_{10}K/T \; x10^{-3}$ lines $= \; ^{-E}/R$ x 2.30 on the
Arrhenius plots, shown in figure 5-3 and 5-4.   The E values
obtained were listed in Table 5-3 and compared with that of
oxidation of carbon in air obtained from the data of Tu, Davis
and Hottel (39).

5-4 Some observations made and discussion of results

5-4-1 Combustion of carbon in air

It is well established that the mechanism of oxidation
of carbon in air depends on the temperature, there being two
mechanisms (10) (39) ; (i) below $1,000^{\circ}K$, the rate process is
controlled by the chemical-reaction of the reactant and the
carbon, where desorption of the reaction products plays a vital
part ; (ii) above $1,000^{\circ}K$, diffusion control prevails, where
not only oxygen diffusion through the boundary layer (39) but

also the adsorption of oxygen by the carbon (10) play vital

parts. The activation energies for these processes reported

in the literature vary somewhat depending upon the types of carbon

used and experimental conditions, etc. However it would seem the

value of E is of the order of 40 Kcal/mol. for the former process

whereas it is below 10 Kcal/mol. for the latter process (10)

(39). The work of Tu, Davis and Hottel (39) seems most widely

quoted in the papers (10) (12) concerning the combustion of car-

bon and has also recently been re-examined and confirmed by Essen-

high, Froberg and Howard (10), who agree that the activation

energy is 35-40 Kcal/mol. for the chemically controlled process

but is reduced to 2-4 Kcal/mol. for the diffusion controlled

process. Hence the results obtained by the author were compared

with those of Tu, Davis and Hottel and plotted together in figure

5-3. The results are in good agreement since the slope of the

curve is similar but the transition range of temperature from one

mechanism to the other is about $100^{\circ}C$ lower in the author's results

as compared to those of Tu, Davis and Hottel. This is most likely

to be due to the fact that the type of carbon employed by the author

was more reactive than Tu's. In detail, a brush carbon of high

grade, having an apparent density of 1.55, was used in Tu's experi-

ment and a highly combustible electrode carbon, having bulk density

of 1.57 was used in the present research.

The activation energies obtained, from the best fitting

straight lines by the author were 31 Kcal/mol. for the chemical-

reaction controlled process and 4 Kcal/mol. for the diffusion con-

trolled process, whereas E values were 35 Kcal/mol. and 2.4 Kcal/mol.

by Tu, Davis and Hottel. This amount of discrepancies is only to be

expected bearing in mind the experimental errors encountered.

5-4-2 Oxidation of carbon in the melts

The oxidation rate of carbon in the melts is plotted in figure 5-2, together with that of carbon in air for comparison. As it can be seen, the rate of oxidation is highest in $NaVO_3$ melt, next to this is $Na_2B_4O_7$ melt and lowest is $Na_2O \cdot 2SiO_2$ melt.

It is interesting to consider if the rate of oxidation in the melts might be related to the viscosity of melts. Thus the viscosity of the melts are listed in Table 5-4 with the rate of oxidation of carbon.

Table 5-4

	Viscosity (poise)			Combustion rate $(gm/cm^2/hr.)$	
	$1,000°C$	$800°C$	Refs.	$1,050°C$	$1,000°C$
$NaVO_3$	0.33	0.46	(11)	–	0.1653
$Na_2B_4O_7$	–	12.76	(11)	–	0.0037
$Na_2O \cdot 2SiO_2$	1318	–	(11)	0.0019	'0.0007'

' ' : by extrapolation

From the table, it is shown that the lower the viscosity, the more oxidized the carbon as far as these melts are concerned. However, the E values for combustion of carbon in melts does not correlate the E values for viscous flow of melts as shown in Table 5-5.

Table 5-5

Melts	$E_{viscous\ flow}$ Kcal/mol.	Refs.	$E_{combustion}$ Kcal/mol.
$Na_2B_4O_7$	56	(35)	23
$NaVO_3$	12.5	(11)	22
Na_2SiO_3	35.5	(2)	24

Turning now to the Arrhenius plots of the oxidation rate
of carbon in the melts shown in figure 5-4, the activation ener-
gies, for the oxidation of carbon in sodium metavanadate, sodium
tetraborate and sodium silicate (in the last case, above $1,150^\circ C$),
are about 22-24 Kcal./mol. which is half way between the value for
the chemical controlled and diffusion controlled processes for
oxidation of the carbon in air. But it is this author's opinion
that it is unsuitable to decide the mechanism of the oxidation of
carbon when immersed in liquid by comparing energies of activation
of the oxidation process with those of carbon in air. Because
empirical E values are obtained from the Arrhenius equation,

$K = A \exp(^{-E}/RT)$, on the assumption that the rate process is

dependant only on temperature. It must not be overlooked that
other factors would be expected to play a part in deciding the
combustion mechanism, in those two processes, namely, the diffusion
rate of oxygen molecules to the carbon, the chemical reaction bet-
ween carbon and oxygen, the formation of reaction products (either
CO or CO_2) and the rate of removal of reaction products away from
the carbon.

But from the fact that the activation energies for the
oxidation process in different melts, are the same (see figure
5-4), it may be assumed that the rate controlling processes are
the same in all reactions. Then this would mean that there was
a common phenomenon prevailing. Before further discussing this
aspect, attention is drawn to the reactivity of carbon in molten
$NaVO_3$ which was found to be vigorous even in the absence of air
above the melt (i.e. nitrogen atmosphere) as can be seen in figure

5-4.   The rate of oxidation (k) in the presence and absence

of air above the melt is tabulated in Table 5-6 together with

the activation energy (E_k) for the oxidation process.

Table 5-6

	Air above the melt		N_2 above the melt	
	K (gm/cm^2/hr.)	E_k	K (gm/cm^2/hr.)	E_k
850	0.0470)		0.0283)	
900	0.0926)		'0.0430')	
		22		21
950	0.1140)		0.0619)	
1,000	0.1653)		'0.1060')	

'   '; by extrapolation

The above table shows the rate is about halved in N_2

atmosphere above the melt compared to the rate in air above the

melt.   It implies the carbon was oxidized directly by the sodium

metavanadate.   Also indicated is that a diffusion controlled rate

process prevailed, since the reaction - rate at the interface varied

with the quantity of oxygen available in the melt. This is the

analogy of the combustion mechanism in air by diffusion controlled

process where the oxygen pressure and air velocity made the rate

different but the E values were the same (39).

It is known that a boundary layer exists in a heterogenous

reaction when the reaction rate is faster than the rate of removal

of the reaction.products.   Considering the reaction between carbon

and oxygen, the reaction products are CO and CO_2.   Then the carbon-

ate anion would be expected to form adjacent to the carbon surface.

And these reaction products will be common to all reactions.   Then

the rate process is likely to be controlled by the carbonate anion-rich boundary layer. If so, the E_k for the oxidation (21 - 24 K cal/mol.) would be near to the $E_{viscous\ flow}$ of the Na_2CO_3 (2). Janz (22) reported that the activation energy for viscous flow of molten sodium carbonate is 26 K cal/ mol. It reinforces the above statement. Hence, it may be stated that the reaction product (CO_3^{-2}) forms a boundary layer around the carbon surface in all oxidation reactions and the rate process of the oxidation of carbon under melts may be controlled here by the diffusion of the carbonate anions through a sodium carbonate rich boundary layer.

The activation energy for the oxidation of carbon in sodium silicate below 1,150°C was 61 K cal/mol. which was much more than that of carbon in the same melt above 1,150°C, 24K cal/ mol. as shown in Table 5-3. It seems that the amount of oxygen available in the melt is diminished considerably below 1,150°C. Then the reaction at the interface is likely to be the rate deter-ming process at this temperature range.

Another interesting fact noticed was the carbon oxidized in a different rate along with the position of carbon submerged in sodium metavanadate melt. The results obtained are listed in Table 5-7 and plotted in figure 5-5. As has been observed by the previous workers (11) (33), the convection of the melt produced by the thermal gradient within the melt was also observed by the author. But while the carbon was submerged, the convection was more violent due to the process of removal of the reaction products. It is likely that the deeper the carbon is submerged, the more convection of the melt is produced. Therefore, more oxygen could

be available as carbon is submerged in deeper position as far
as highly convecting melt is concerned, such as sodium
metavanadate. However, the results may be reversed if the
carbon is submerged in a highly viscous melt with none or less
convection, such as sodium silicate.

Table 5-7   The oxidation rate of carbon in $NaVO_3$ melt in
different positions at $900^{\circ}C$.

Depth of carbon below the surface(cm)	Oxidation rate $gm/cm^2/hr.$
2.3	0.0592
4.3	0.0724
6.3	0.0953

Chapter 6

Corrosion results and sources of errors.

Chapter 6   Corrosion results and sources of errors

6-1   Calculation of results

6-1-1   Density of melt

The density of melt was measured as described in section 4-4-1 and calculated as follows ;

$$D_{melt} = \frac{Wa - Wm}{Vp \; x \; Et} \quad gm/ml.$$

Wa : Weight of platinum sphere in air

Wm : Weight of platinum sphere in melt

Vp : Volume of platinum sphere at $20^{o}C$

Et : Volume expansion of platinum sphere

at the temperature of melt

The thermal expansion of platinum (Et) was obtained from the data collected by White (43). The expansion data used, is given in Table 6-1.

The density of molten sodium borate against temperature is plotted in figure 6-13 together with the density obtained by Safdar (33).

6-1-2   Weight loss of specimen from weight change on balance

$$Weight \; loss \; of \; specimen = \frac{Wb}{1 - Dm/Ds}$$

Wb : weight change on balance
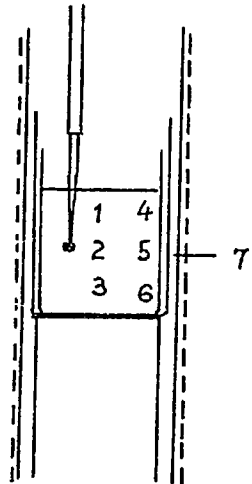
Dm : density of melt

Ds : density of specimen

6-2   Sources of errors

6-2-1   Temperature measurement

For accurate temperature measurement, a bare thermocouple was put into the melt as shown in a schematic diagram given below. To find out temperature gradient within the melt, temperature of various positions in the melt was determined and given below ;

Position	Temperature ^{o}C
1	920
2	919
3	919
4	923
5	926
6	926
7	996

The error due to temperature measurement was estimated as follows : -

Temperature variation in the melt	$\pm$ 3°C
Accuracy of thermocouple	$\pm$ 1°C
Accuracy of potentiometer	$\pm$ 1°C

Consequential percentage weight loss within $\pm$ 5°C is 3%.

6-2-2   Area measurement

The geometrical surface area of specimen was measured by counting the area of the specimen pressed on graph paper. The area occupied more than half of the small squares were counted and those less than half were neglected by visual judgement. The reproducibility was found to be within $\pm$ 1%.

Weight loss, gm.

Specimen No.	after once cleaned	after twice cleaned	after three times
1	0.0461	0.0465	0.0466
2	0.0502	0.0504	0.0504
3	0.0533	0.0536	0.0535

Maximum error is within the range of 1%.

6-2-4 Composition of melt

To minimize the effect of dissolved refractory in the melt in successive measurements, when a maximum of 1.0 weight % of refractory had dissolved, the melt was changed. No attempt will be made to estimate the error in this respect. However, Safdar (33) reports that the weight loss due to this effect will be decreased in the order of 2%.

6-2-5 Constant error

All previous workers who employed metal holders for a refractory specimen in molten slag revealed enchanced corrosion in the vicinity of metallic contact. Faruqi (11) used the same pattern of platinum holder as in the present research and estimated experimentally the increased amount due to the holder as about 5.5%. This % of increased corrosion is reproducible.

6-2-6 Summation of errors

Sources of error	Estimated error
Temperature	3%
Area	1%
Weighing	1%
Total possible error	5%
Platinum contact - constant error	5.5%

6-3 Results

(All calculations were done by the calculating machine supplied by Industria Macchine Elettroniche - model 86 S.)

Table 6-1   The volume expansion of platinum

Temperature, $^{\circ}$C	Et
0	1.00000
800	1.02379
900	1.02696
1,000	1.03033
1,100	1.03385

Table 6-2   Dissolution of sapphire in $Na_2B_4O_7$ melt

(by continuous weighing technique)

Weight loss (gm/cm^2)

Time (min.)	900°C	950°C	1,000°C
1	0	0	0
2	0.0015	0.0017	-
3	-	-	0.0033
5	0.0034	0.0043	0.0055
10	0.0058	0.0072	0.0096
20	0.0102	0.0129	0.0185
30	0.0135	0.0214	0.0270
60	0.0234	0.0344	0.0479

Table 6-3 Dissolution of single crystal of MgO in $Na_2B_4O_7$ melt

(by continuous weighing technique)

Weight loss (gm/cm^2)

Time (min.)	$900^{\circ}C$	$950^{\circ}C$	$1,000^{\circ}C$
1	0	0	0
2	0.0009	0.0013	0.0017
3	0.0020	0.0025	0.0043
5	0.0027	0.0049	0.0085
10	0.0056	0.0108	0.0186
15	0.0082	0.0174	0.0134
20	0.0115	0.0230	0.0424
30	0.0168	0.0355	0.0638
60	0.0334	0.0740	0.1264

Table 6-4 Dissolution of 29% porous alumina in $Na_2B_4O_7$ melt

(by static corrosion technique)

Weight loss (gm/cm^2)

Time (min.)	$900^{\circ}C$	$950^{\circ}C$	$1,000^{\circ}C$
4	0.0207	0.0253	0.0297
8	0.0245	0.0288	0.0328
15	0.0278	0.0355	0.0395
30	0.0364	0.0453	0.0502
60	0.0415	0.0574	0.0708
120	0.0572	0.0829	0.1039
180	0.0699	-	-

Table 6-5   Corrosion of carbon-containing alumina (deposited

from pitch) and corresponding 29% porous alumina

in $Na_2B_4O_7$ melt at $900^\circ C$. (nitrogen atmosphere)

Weight loss(gm/cm^2)

Time (min.)	29% porous alumina	3.7% carbon-containing alumina	6.8% carbon-containing alumina
4	0.0207	0.0114	0.0067
8	0.0245	· 0.0127	0.0122
15	0.0278	0.0182	0.0127
30	0.0364	0.0218	0.0181
60	0.0415	0.0347	0.0247
120	0.0572	0.0464	0.0388
180	0.0699	-	0.0421

Table 6-6   Corrosion of carbon-containing alumina and

corresponding 29% porous alumina in $Na_2B_4O_7$ melt

at $950^\circ C$ (nitrogen atmosphere)

Weight loss (gm/cm^2)

Time (min.)	29% porous alumina	4.7% carbon-containing alumina	3.5% carbon-containing alumina
4	0.0253	0.0157	-
8 ·	0.0288	0.0221	0.0071
15	0.0355	0.0297	-
30	0.0453	0.0419	0.0232
60	0.0574	0.0495	0.0256
120	0.0829	0.0727	0.0392
		(pitch)	("Cascote"resin)

Table 6-7   Corrosion of carbon-containing alumina (deposited

from pitch) and corresponding 29% porous alumina

in $Na_2B_4O_7$ melt at $1,000^{\circ}C$ (nitrogen atmosphere)

Weight loss (gm/cm^2)

Time (min.)	29% porous alumina	carbon-containing alumina		weight % of carbon
4	0.0297	0.0155	–	(5.24)
8	0.0328	0.0297	–	(5.20)
15	0.0395	0.0340	–	(5.27)
30	0.0502	0.0460	–	(5.16)
60	0.0708	0.0611	–	(5.23)
120	0.1039	0.0860	–	(4.96)

Table 6-8   Corrosion of 21% porous alumina in $NaVO_3$ melt

Weight loss (gm/cm^2)

Time (min.)	$850^{\circ}C$	$950^{\circ}C$
4	–	0.0054
15	0.0031	–
30	0.0067	0.0274
60	0.0089	0.0450

Table 6-9   Corrosion of carbon-containing alumina and corresponding 21% porous alumina in NaVO$_3$ melt at 850°C. (nitrogen atmosphere)

Weight loss (gm/cm^2)

Time (min.)	21% porous alumina	2.4% carbon- containing alumina
4	–	0.0042
15	0.0031	0.0104
30	0.0067	0.0131
60	0.0089	0.0254

Table 6-10   Corrosion of carbon-containing alumina (deposited from pitch) and corresponding 21% porous alumina in NaVO$_3$ melt at 950°C (nitrogen atmosphere)

Weight loss (gm/cm^2)

Time (min.)	21% porous alumina	2.4% carbon- containing alumina	
4	0.0054	0.0133	0.0098
15	–	0.0374	–
30	0.0274	0.0454	0.0490
60	0.0450	0.0970	0.0932
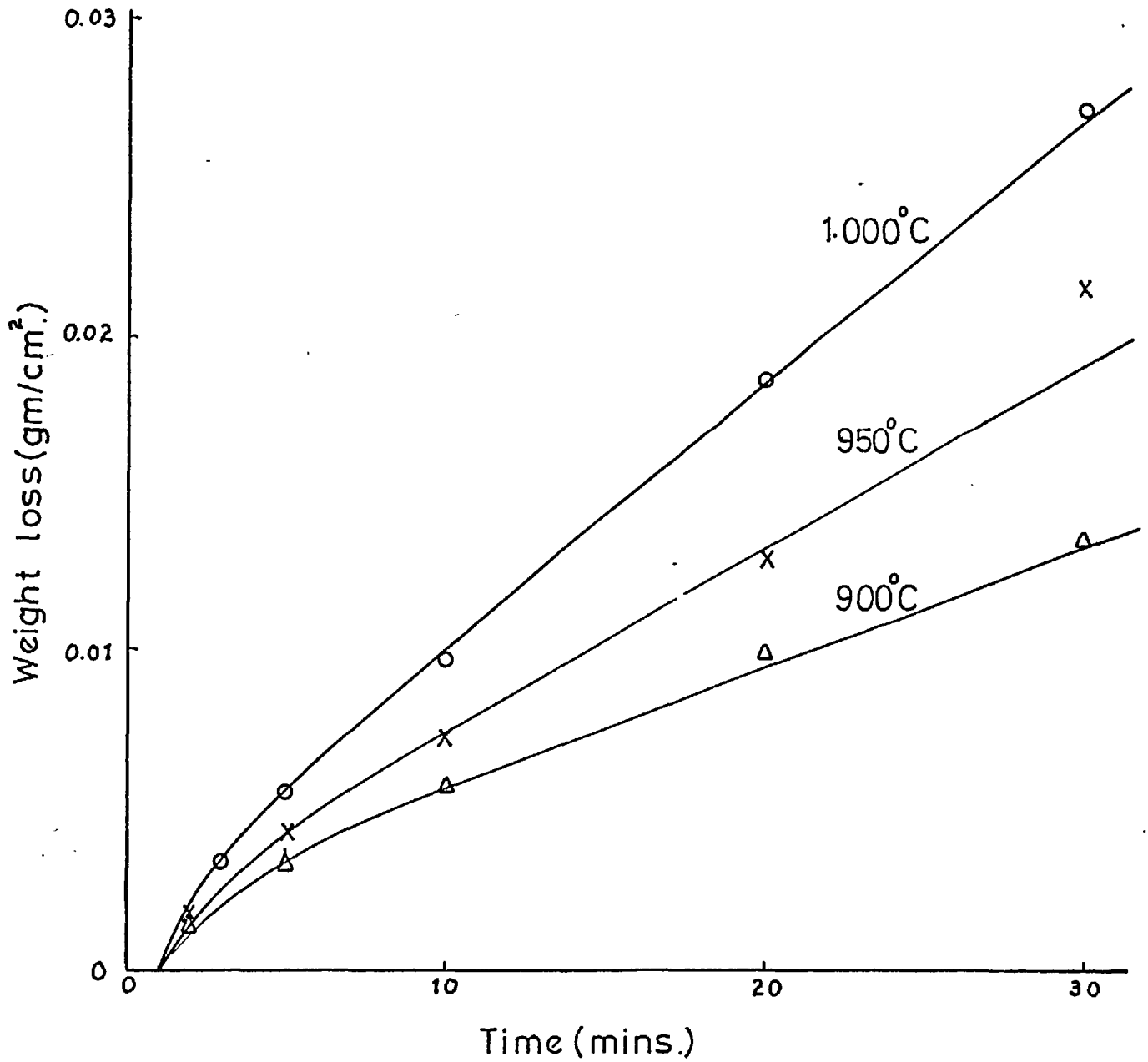
Figure 6-1 Corrosion of sapphire in sodium tetraborate.
(continuous weighing technique)
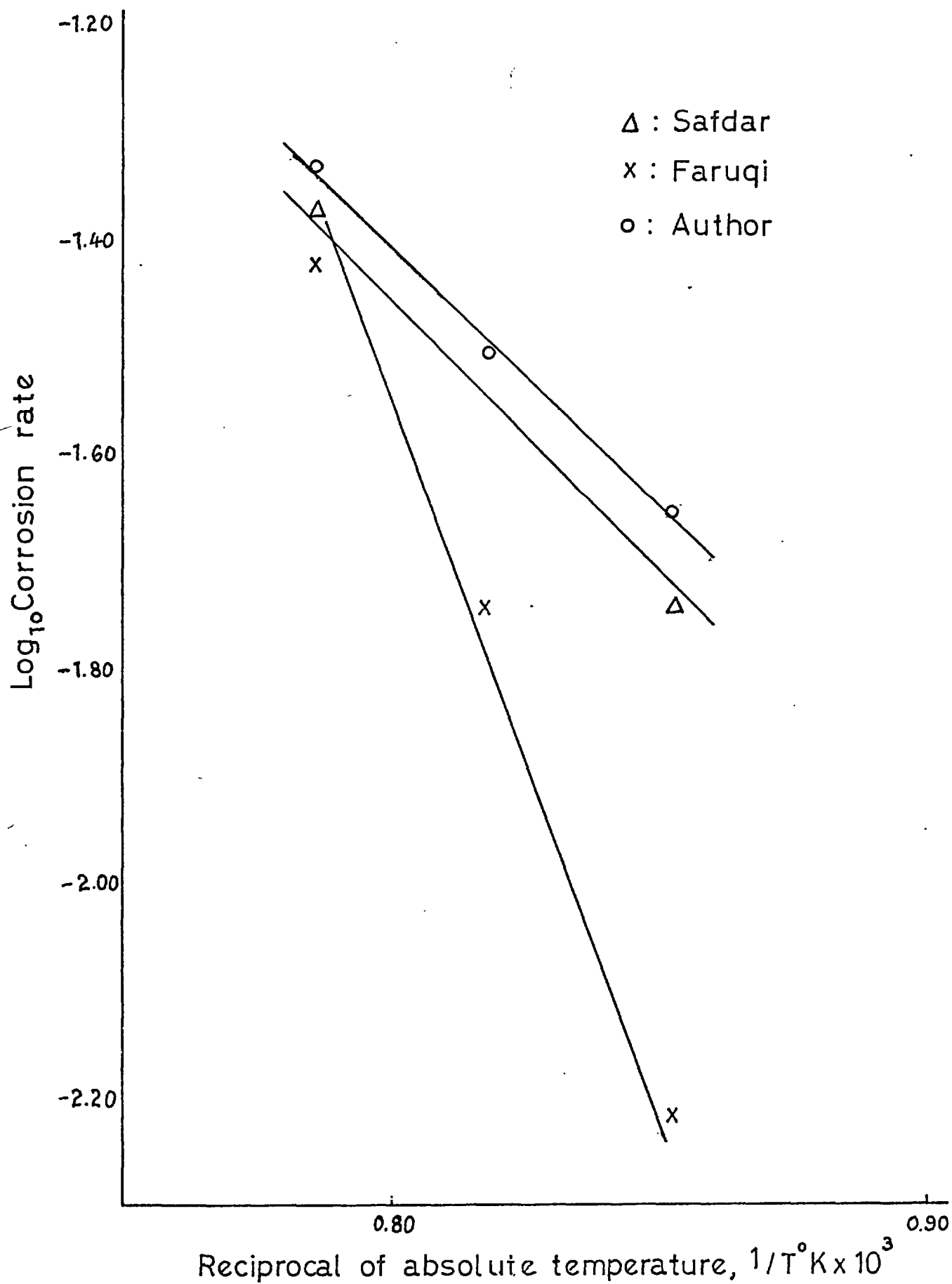
Figure 6-2   Arrhenius plot of the steady state corrosion
rate of sapphire in sodium tetraborate.
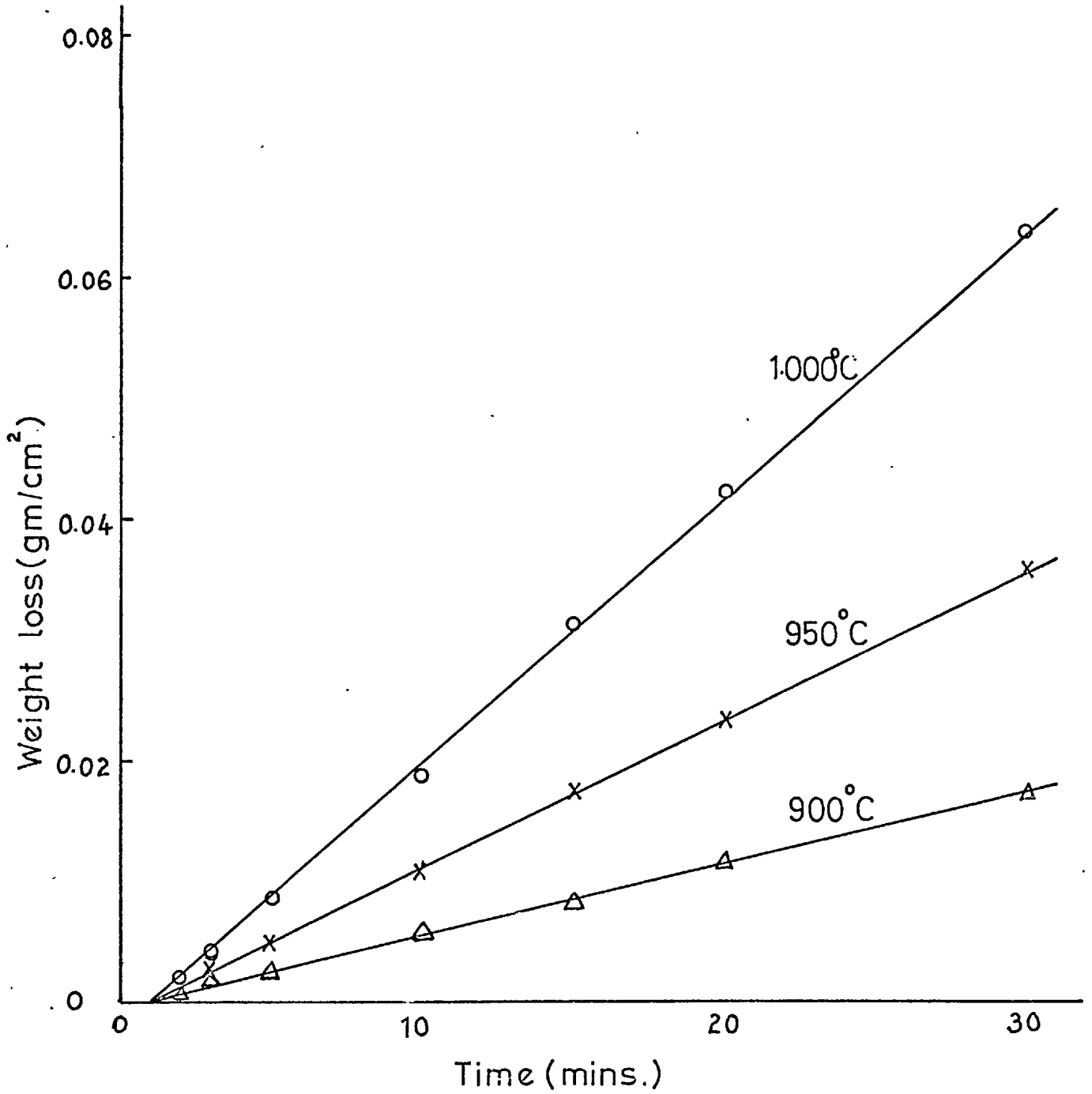
Figure6-3 Corrosion of magnesia single crystal in sodium tetraborate (continuous weighing technique)
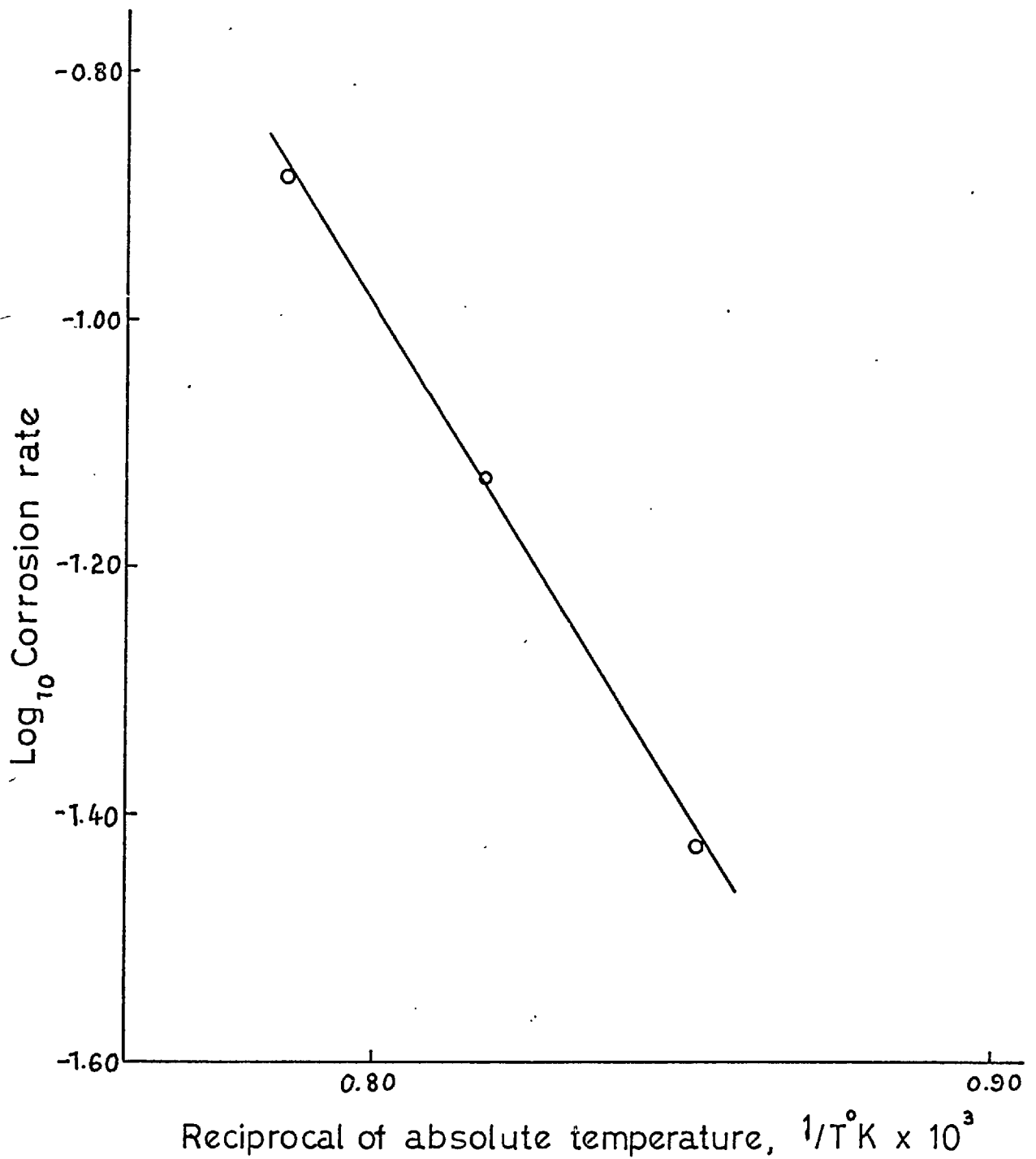
Figure 6-4   Arrhenius plot of the rate of corrosion of magnesia single crystal in sodium borate.
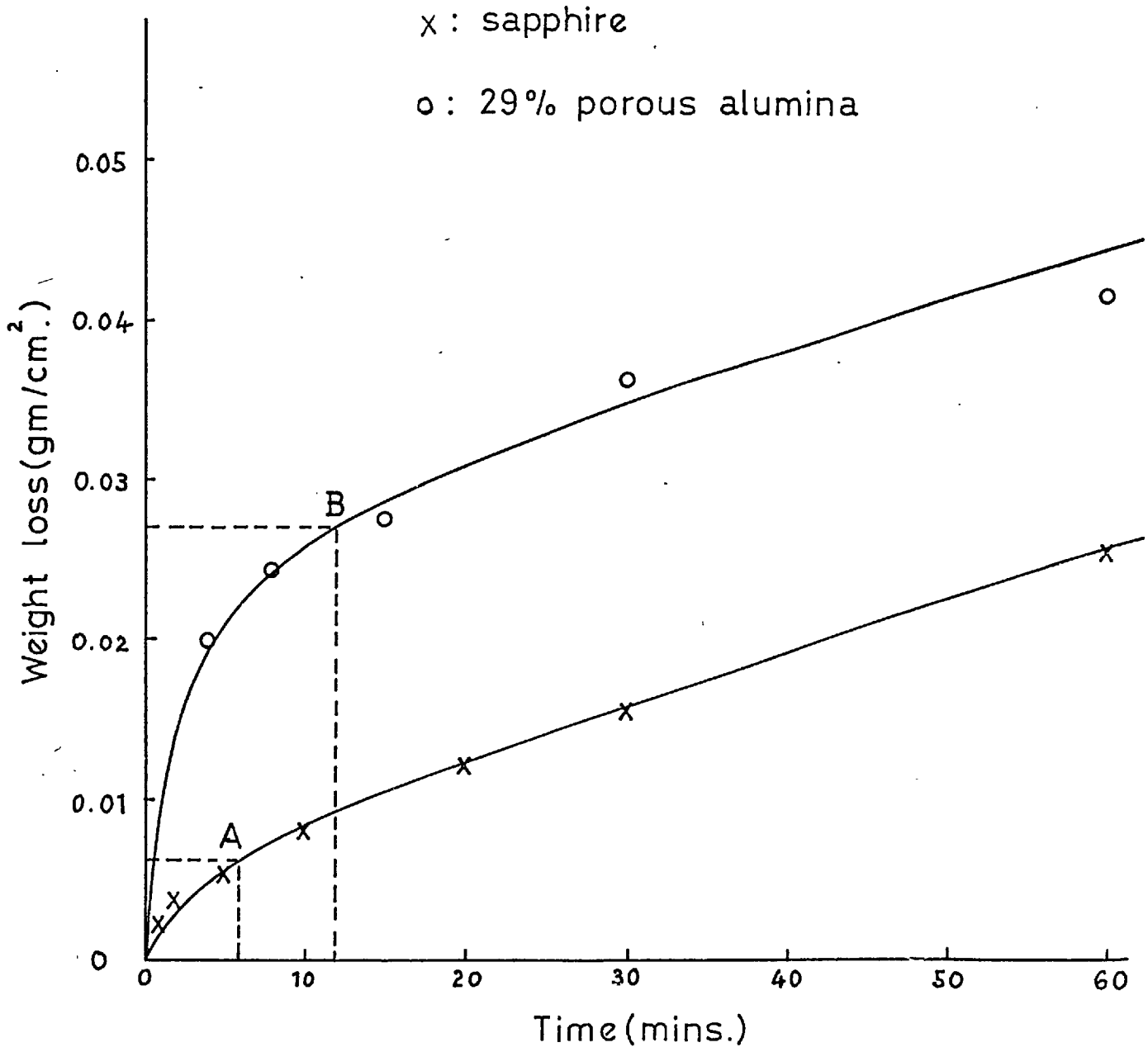
Figure 6-5 Corrosion of sapphire and porous alumina
in sodium tetraborate at 900°C.
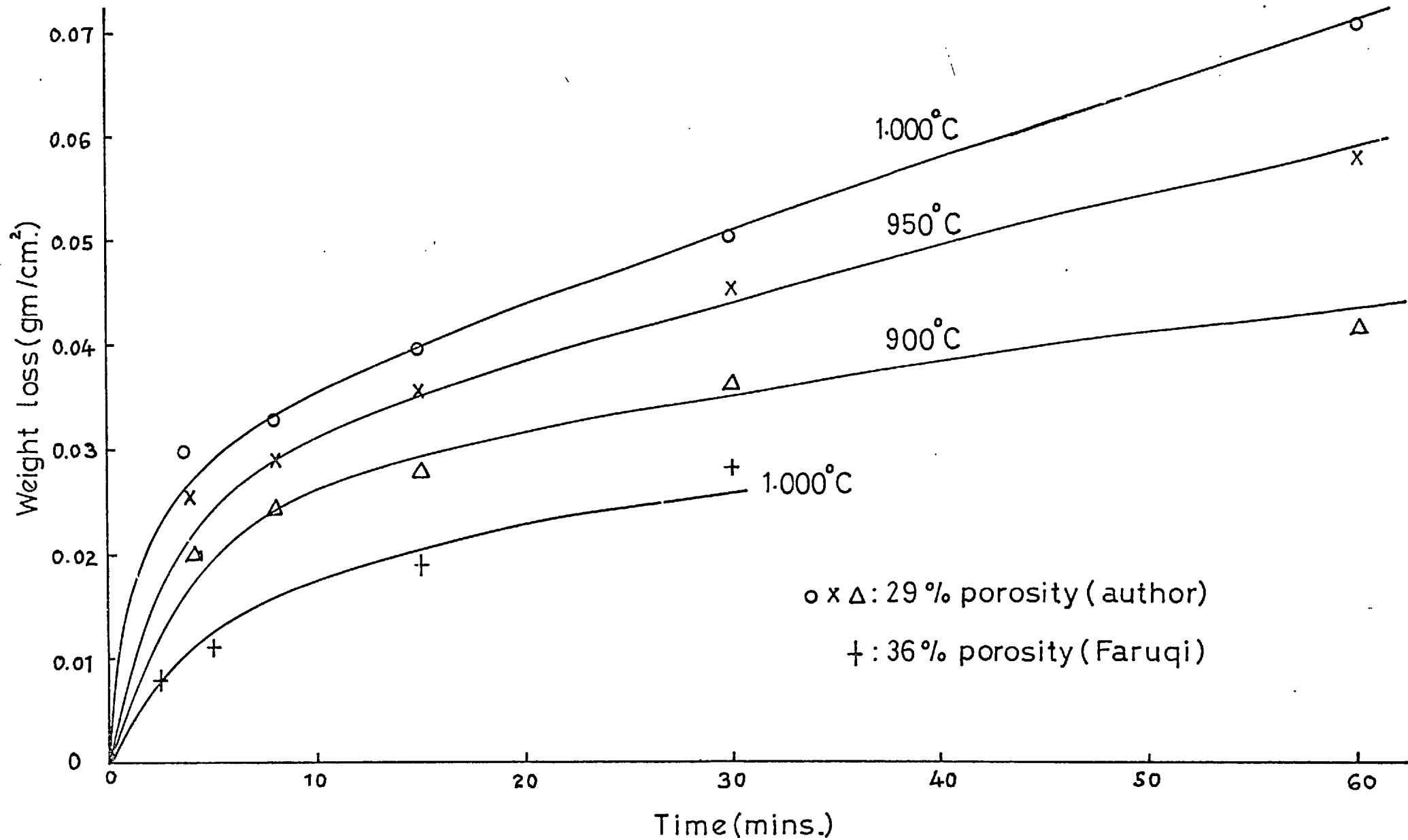
Figure6-6 Corrosion of porous alumina in sodium tetraborate.

x : 3.7 W/o carbon-containing alumina(pitch)

△ : 6.8 W/o carbon-containing alumina(pitch)

o : corresponding 29% porous alumina

Figure 6-7 Corrosion of carbon-containing alumina in sodium tetraborate at 900°C .

x : 4.7 W/o carbon-containing alumina (pitch)
+ : 3.5 W/o carbon-containing alumina (resin)
o : corresponding 29% porous alumina
Δ : sapphire
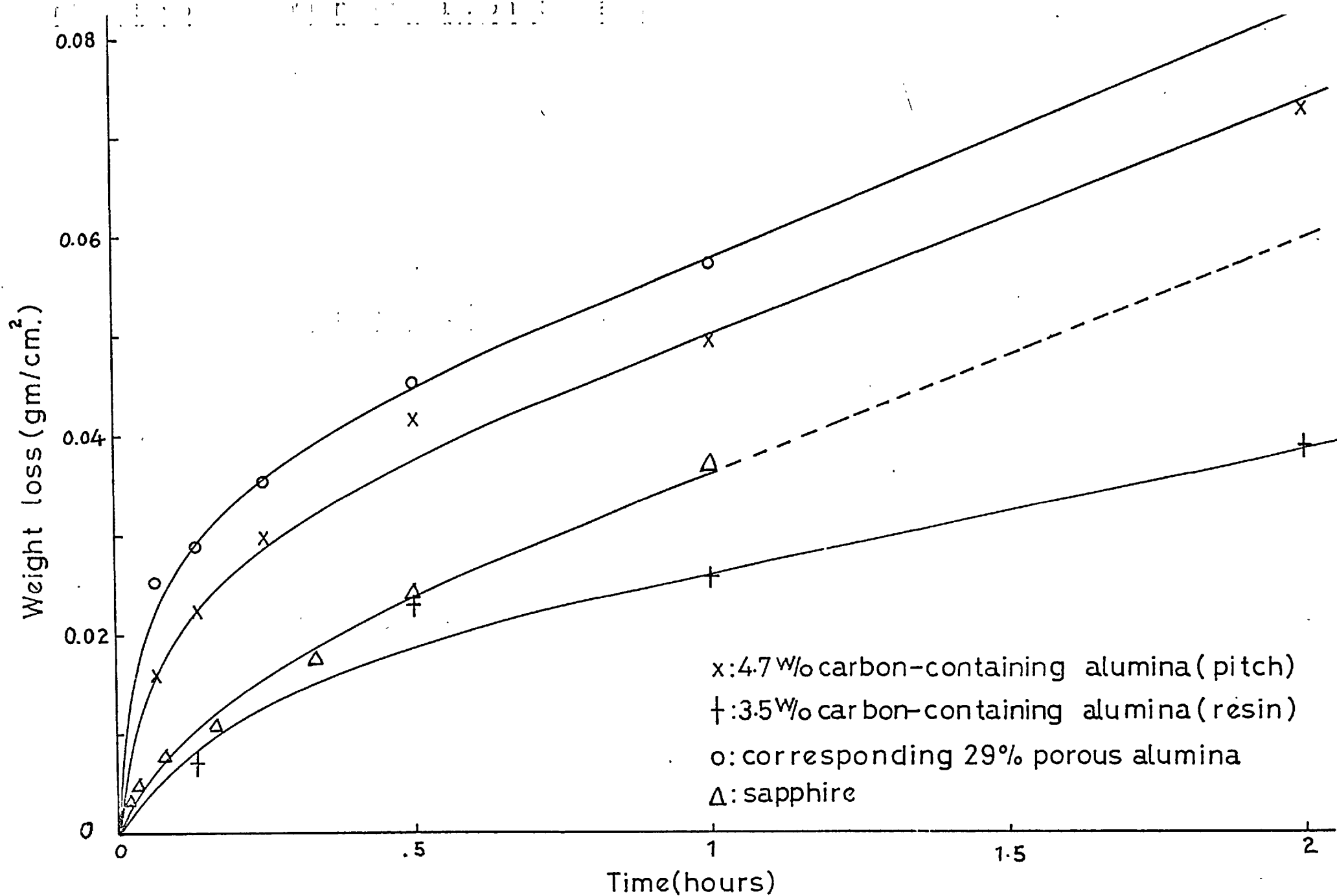
Figure 6-8   Corrosion of carbon-containing alumina in sodium tetraborate at 950°C.

x : 5.1 W/o carbon-containing alumina (pitch)

o : corresponding 29% porous alumina
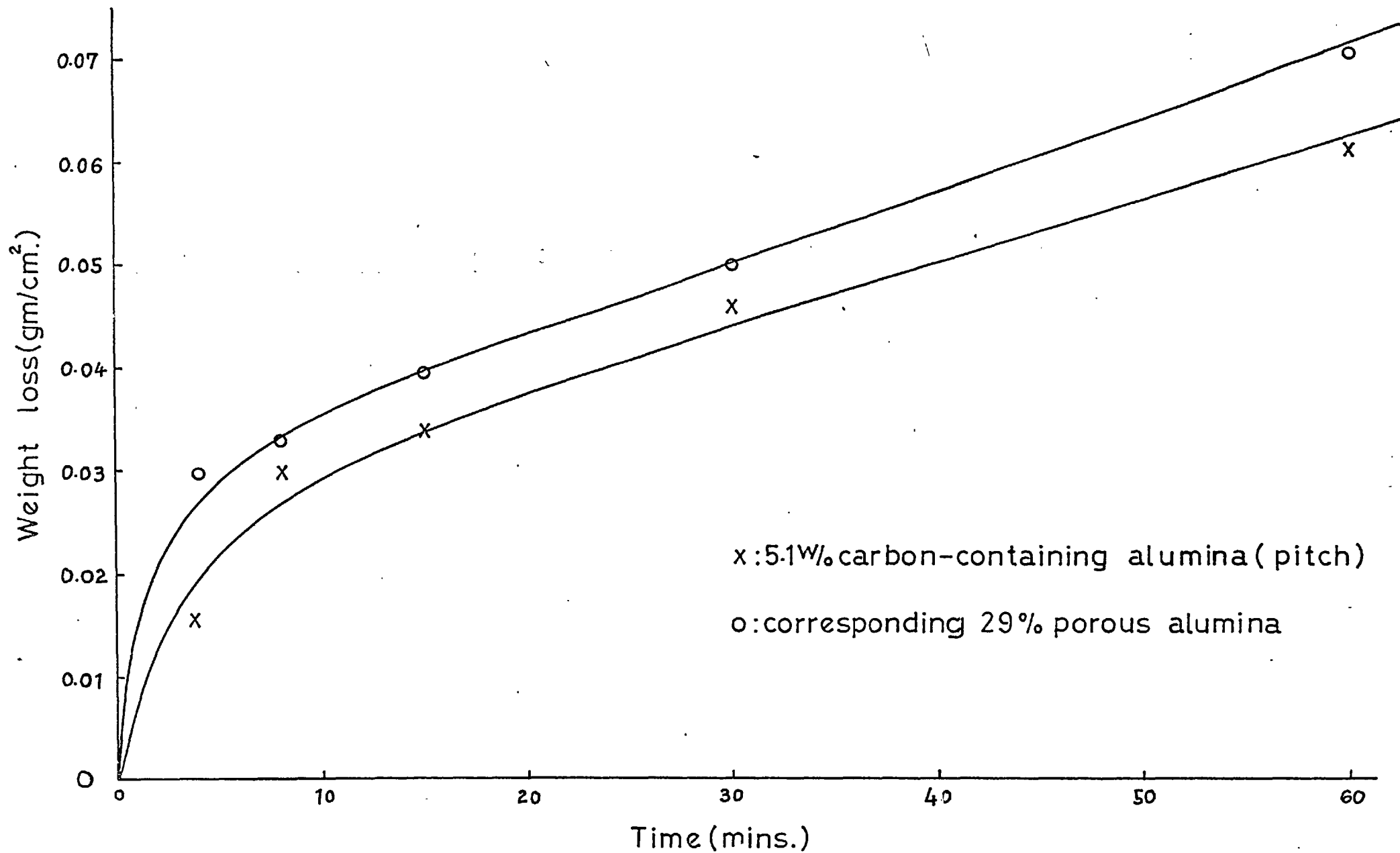
Figure 6-9   Corrosion of carbon-containing alumina in sodium tetraborate at 1.000°C.
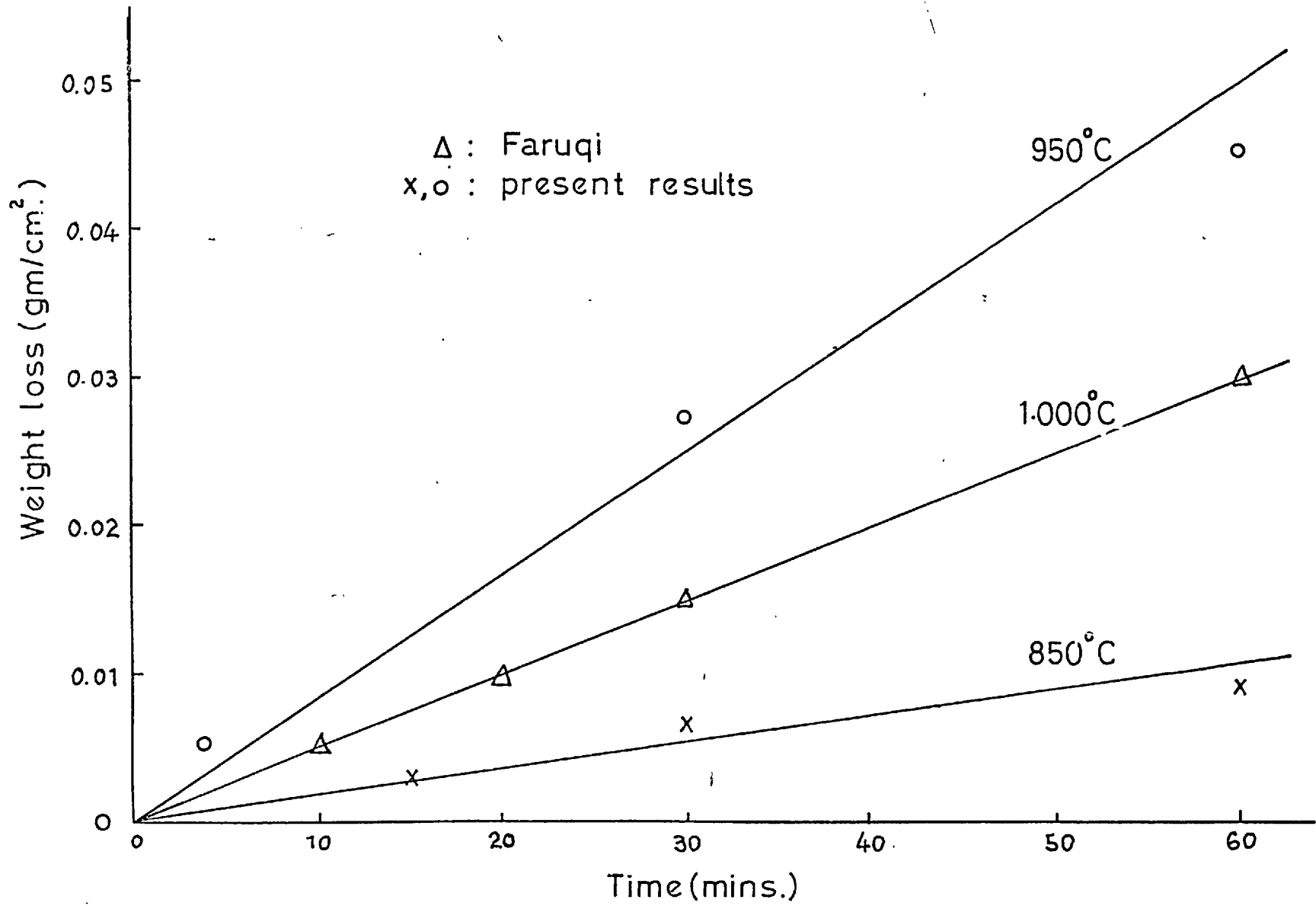
Figure 6-10   Corrosion of 21% porous alumina in sodium metavanadate.
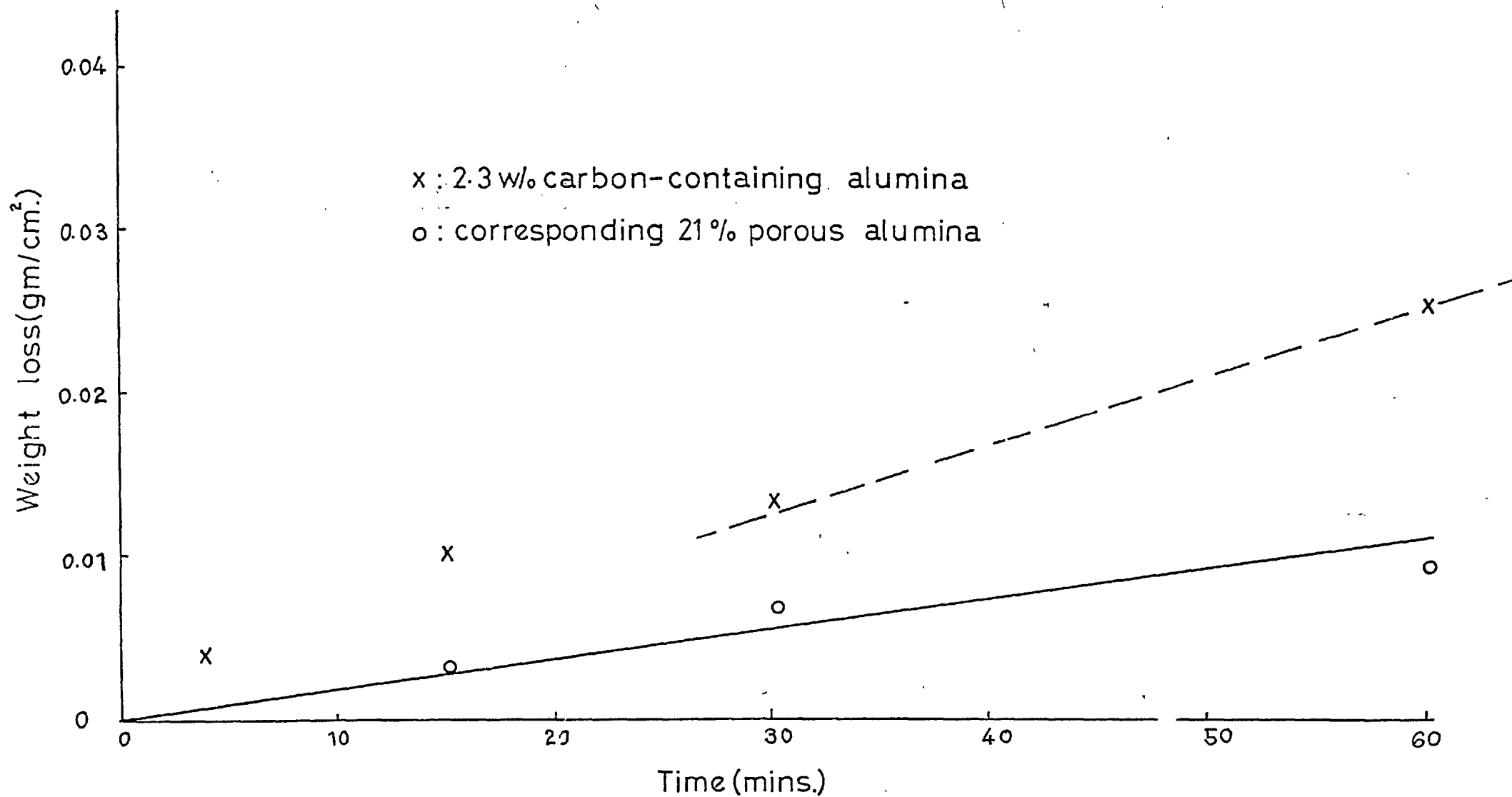
Figure 6-11 Corrosion of carbon-containing alumina in sodium metavanadate at 850°C.
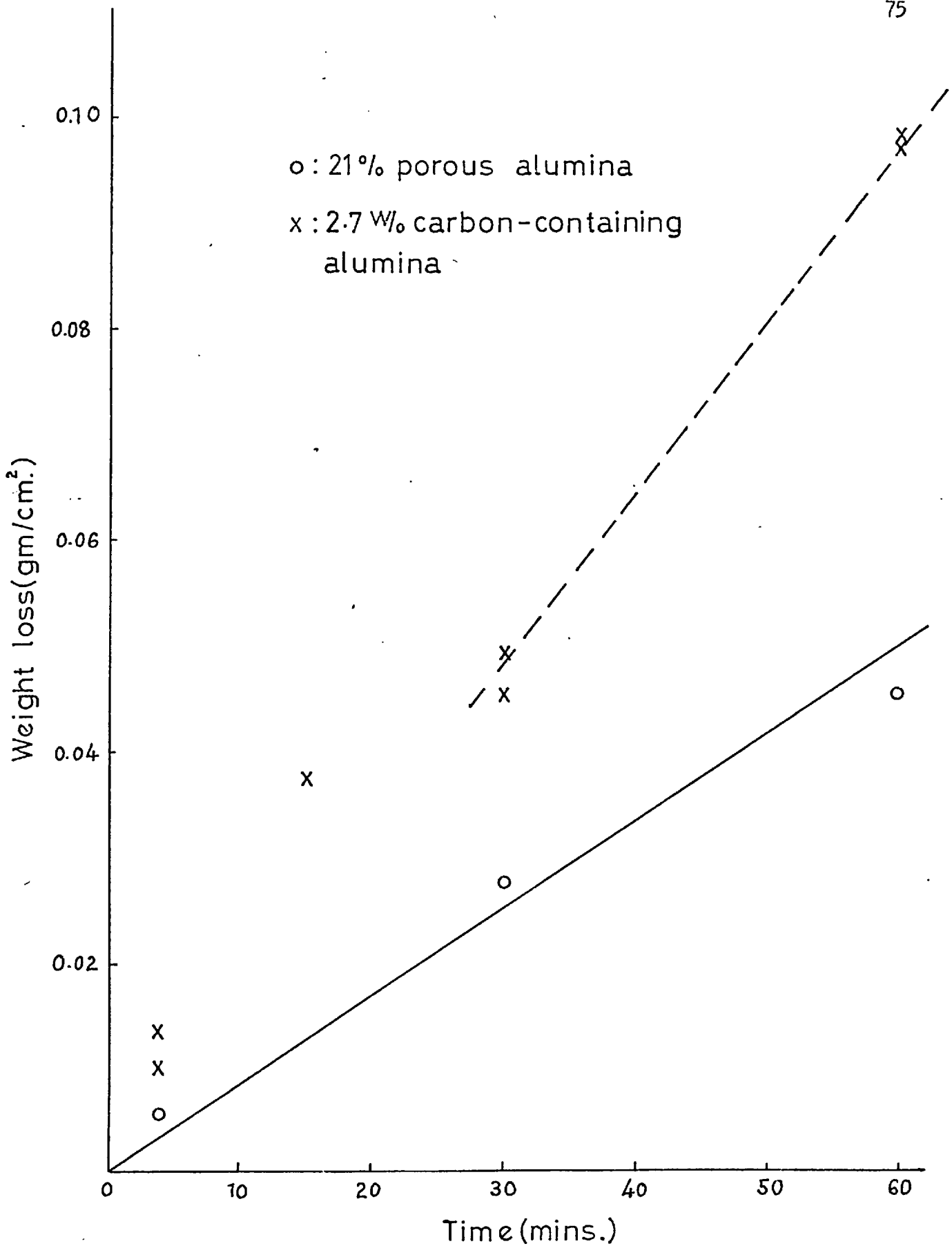
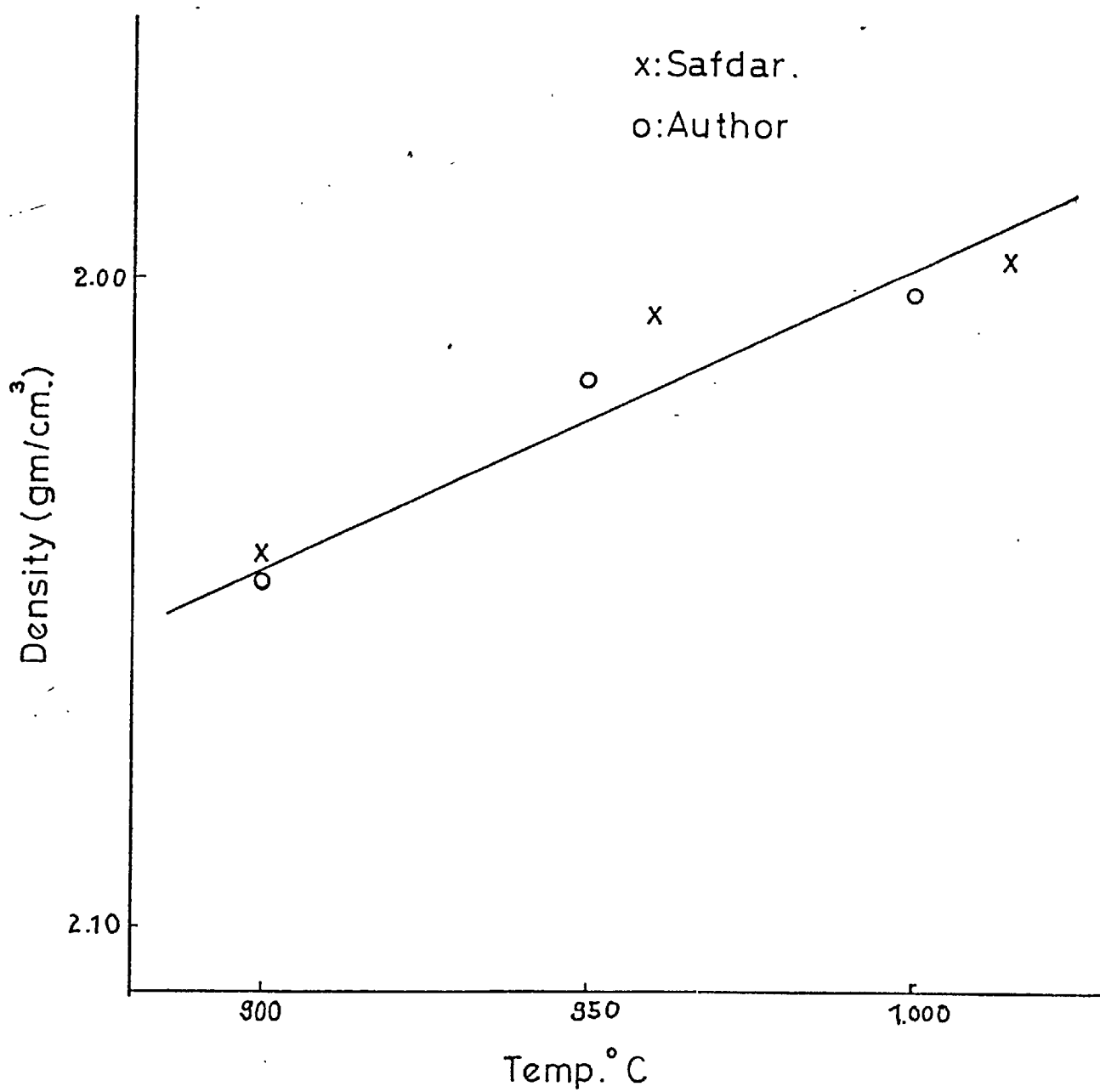Figure 6-12 Corrosion of carbon-containing alumina in sodium metavanadate at 950°C.
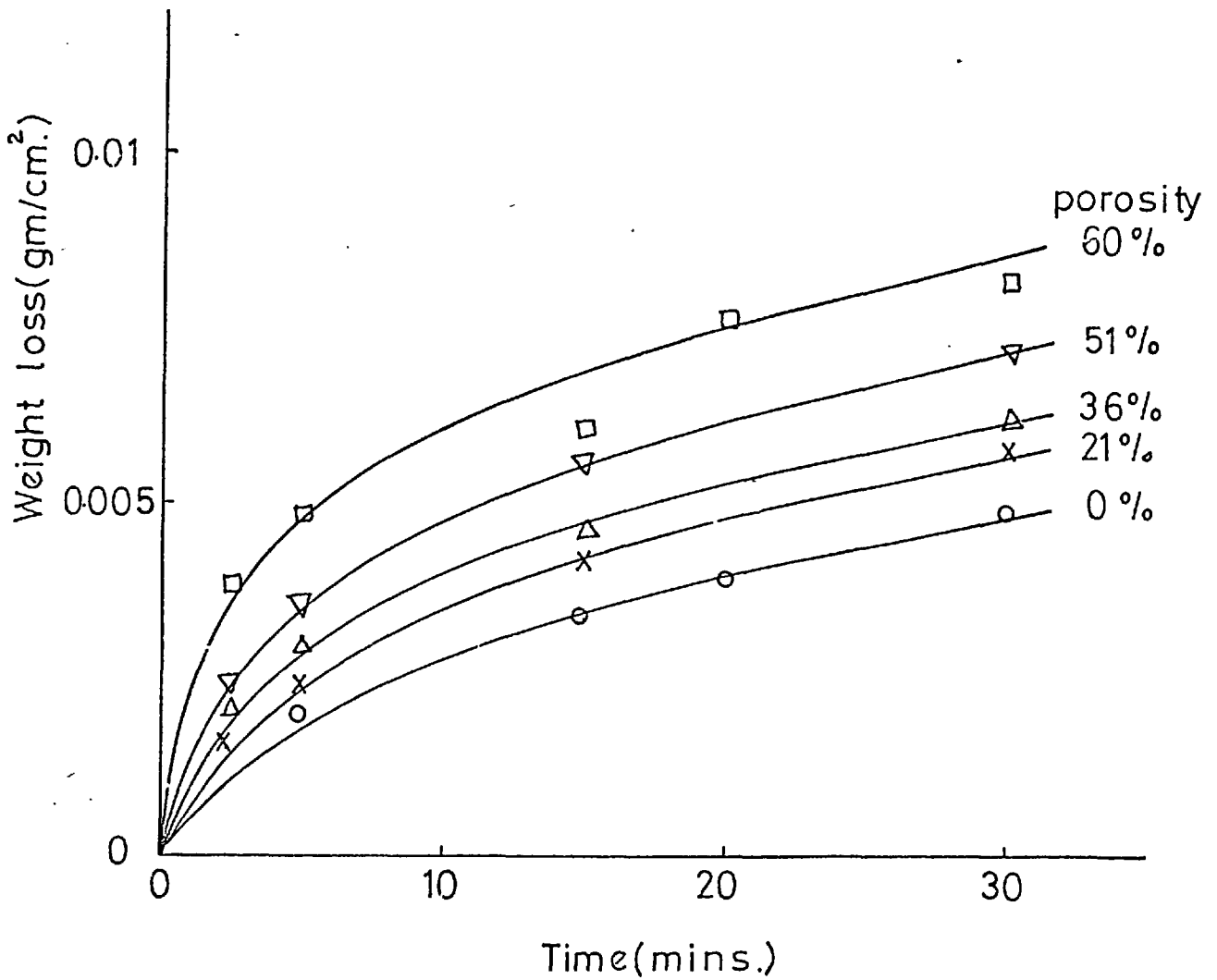
Figure 6-13   Density of sodium tetraborate.

Figure 6-14   Corrosion of porous alumina in sodium
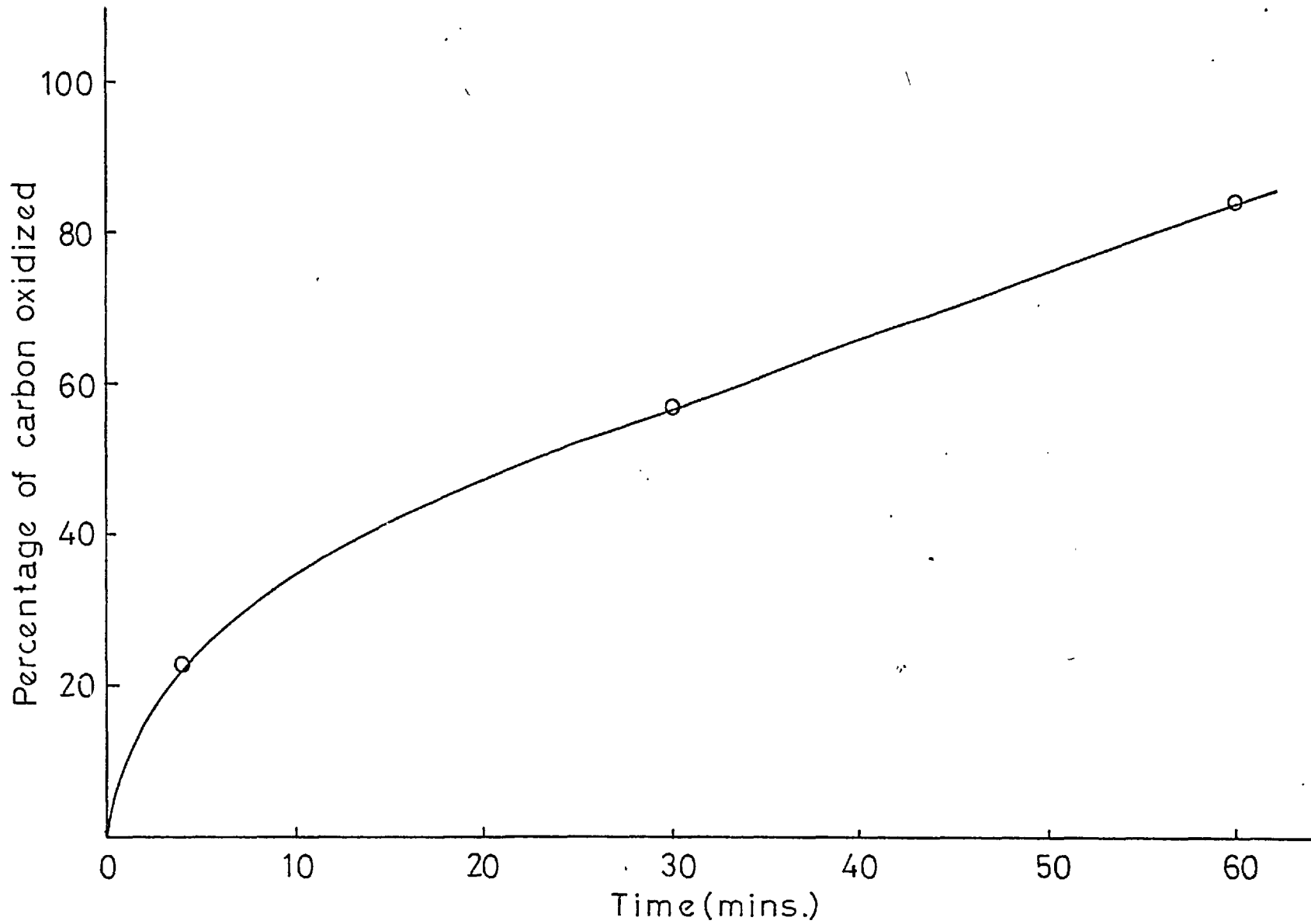   tetraborate at 900°C(Faruqi)

Figure 6-15   Percentage of carbon oxidized (deposited in the pores) versus time in sodium metavanadate at 950°C.

Chapter 7

Discussion of results.

Chapter 7   Discussion of results

Preliminary work was carried out with alumina and mag-
nesia in the form of single crystals and transparent silica

glass. These were submerged in sodium tetraborate or sodium

metavanadate melt in order to confirm the mechanism of corro-

sion.   In fact either the slagging mechanism was fairly well

established by previous workers or the mechanism could be pre-

dicted from the results obtained by previous workers, McCallum

(26), Reed (30), Faruqi (11), Safdar (33) and Barham (2).

Next, attention was given to the effect of porosity of

the refractory oxide with respect to the corrosion resistance

in melts before tackling the case of carbon-containing refractory

oxide, bearing in mind that carbon will be deposited in the pores

of refractory oxides.

The detailed discussion on above aspects will be discussed

first, based on the results obtained by this author in comparison

with the results obtained by previous work-ers and followed by the

discussion on the corrosion resistance of carbon-containing alumina,

with respect to the effect of carbon, in sodium tetraborate and

sodium metavanadate.

7-1   The dissolution of refractory oxides in melts

7-1-1   Alumina (sapphire) in sodium tetraborate

Figure 6-1 shows typical weight loss/unit area versus time

curve of sapphire dissolving in non-silicate glass melt, namely

sodium tetraborate ($Na_2B_4O_7$), by the continuous weighing technique.

As can be seen, the curve is parabolic during the initial stages of

dissolution.   The first point on the weight loss curve was obtained

two minutes after the sapphire crystal was submerged in the melt,
because of the experimental difficulties as mentioned earlier.
This parabolic shape of the curve was shown by previous workers
(2) (11) (30) (33) as an indication of the time taken to
build up the diffusion layer (or boundary layer) of the reaction
products. This assumption was previously confirmed by rotating
the refractory in the melt (31). Increase of rotation speed
increased the amount weight loss, because there would be a thinner
and thinner diffusion layer built up while the refractory specimen
was rotated faster and faster in melt. Once the diffusion layer
is set up, the curve is changed to straight line. This is an
indication of refractory dissolving at a steady rate, with the
reaction of nearly saturated melt adjacent to the refractory in
melt.

The Arrhenius plot of the rate of corrosion is plotted in
figure 6-2, together with the corrosion rate data obtained by
Faruqi (11) and Safdar (33). It shows a straight line relation-
ship which indicates that the corrosion process follows the
Arrhenius equation (26), $K = A \exp (^{-E}/RT)$. The activation
energy obtained for this process is tabulated below and the E
values compared with those obtained by Faruqi and Safdar.

Corrosion rate of alumina, $gm/cm^2/hr$.

Temperature,^{o}C	Faruqi	Safdar	Author
900	0.0060	0.0180	0.0220
950	0.0180	-	0.0310
1,000	0.0378	0.0423	0.0466
Activation	energy,	K cal/mol.	
62	23	20	

As it can be seen from the plot and table, the E value

20 K cal/mol. obtained by this author agrees well with the E

value obtained by Safdar (33), 23K cal/mol., but disagrees

with that of Faruqi (11), 62 Kcal/mol.   It may be that the

E value obtained by Faruqi is subject to some chance error,

bearing in mind that it is based on only three temperatures.

The following table shows the value of $E_{corrosion}$ $(E_k.)$

compared with the $E_{viscous\ flow}$ $(E_v.)$ of $Na_2B_4O_7$, calculated

from the viscosity data of Shartsis, Capps and Spinner (35),

the value for $E_{conductance}$ obtained from Mackenzie (24) and

bond strengths of Al - O (37).

E_k of Al_2O_3	E_c of $Na_2B_4O_7$	E_v of $Na_2B_4O_7$	Al - O bond
K cals.	K cals	K cals.	K cals.
20	20 - 22	56	79 - 101

From the above table, it may be expected that the dissolu-

tion phenomenon may be controlled by the same mechanism as the

conduction of $Na_2B_4O_7$, i.e. the cation movement, since the value

of E_k and $E_{cond.}$ are similar (33)   meanwhile it is suggested

(2) that one would only expect that the mechanism is to be the

same if the value of $E_{cond.}$ of the saturated melt with Al_2O_3 is

similar to the value of E_k of Al_2O_3 for which data was not available.

However, it is doubtful whether one can derive a useful conclusion

with any degree of certainty from the values of activation energy

listed above, because the E values of conductance and viscous flow

are for the single process (24) (35), being respectively either

cation or anion movement, whereas the value $E_{corrosion}$ represents

the energy required for a complex transport phenomenon, refractory-

melt.

7-1-2 MgO single crystal in sodium tetraborate

The values of weight loss/unit area of magnesia in sodium tetraborate melt, from two to sixty minutes, are listed in Table 6-3 and plotted as a function of time in figure 6-3. As clearly can be seen, it shows a straight line relationship with no indication of parabolic nature as the curve of alumina corrosion in $Na_2B_4O_7$ has shown. Hence it indicated (11) (33) that the mechanism of dissolution is controlled by chemical - reaction at the interface of MgO - $Na_2B_4O_7$ melt.

The Arrhenius plot for this process is shown in figure 6-4 and the activation energy of 37 K cal/mol. was obtained. The values of $E_{corrosion}$ is presented below again with the values of $E_{conductance}$ of $Na_2B_4O_7$ (24), $E_{viscous flow}$ of $Na_2B_4O_7$ (33) and bond strengths of Mg - O (37).

E_k of MgO	E_c of $Na_2B_4O_7$	E_v of $Na_2B_4O_7$	Mg - O bond strengths
K cals.	K cals.	K cals.	K cals.
37	20 - 22	56	37

It is shown that the value of $E_{corrosion}$ (E_k) of 37 K cals. is the same as the bond strengths of Mg - O. Thus it suggests (2) that the mechanism of dissolution appears to be controlled by the disruption of Mg - O bonds in magnesia crystal lattice.

7-1-3 Alumina in sodium metavanadate melt

It was established by Faruqi (11) and further confirmed by Safdar (33) that the corrosion of alumina in molten sodium meta-vanadate is a chemically controlled process. In this instance, the plot of weight loss/unit area as a function of time gives a linear relationship as in the case of MgO corroded by molten $Na_2B_4O_7$.

Also found by Faruqi was the fact that the corrosion rate does not increase with varing rotation velocity of the alumina rod which confirms that the diffusion layer does not exist.

The activation energies for the corrosion obtained by Faruqi and Safdar are 11 K cal/mol. and 17.5 - 21 K cal/mol., respectively. Although the values vary somewhat, both workers agree that the process is unlike an anionic diffusion controlled process. However, Frauqi concluded that the process is likely to be proceeded by a cationic movement in the melt whereas Safdar suggested that the process appears to be related to the mechanism of fusion of alumina since the energy for this process is 26 Kcal/mol.

Although present work has not included the corrosion of single crystal (sapphire) in the melt, the corrosion of 21% porous alumina was performed at $850^{\circ}C$ and $950^{\circ}C$ and presented in Table 6-8 and plotted in figure 6-10 together with the value of weight loss/unit area obtained by Faruqi (11). As in the case of porous alumina in molten sodium borate, the values of weight loss/unit area obtained in the present work are greater than the values obtained by Faruqi, i.e. the wight loss of 21% porous alumina in the melt at $950^{\circ}C$ was 0.045 $gm/cm^2/hr$. by this author whereas 0.030 $gm/cm^2/hr$. at $1,000^{\circ}C$ by Faruqi. Since this discrepancy in the weight loss values is consistent, there should be either consistently different experimental conditions or factors in the material employed, i.e. the position of crystal submerged in the melt, the measurement of temperature or the distribution of pore size.

During the course of experiments, it was found that the corroded porous alumina in the melt disintegrated during the

cleaning procedure in hot diluted HCl solution. This particular

problem was overcome by collecting the disintegrated particles on

a filter paper. The reason for this disintegration may lie in

the complex phenomena of the penetration of the melt. It was

thought that if the reason is due to different thermal expansion

co-efficient between the alumina and the adhered melt on the

specimen or the penetrated melt through the pores, then one would

expect cracking of the test piece while it cools down rather than

disintegrating of the test piece while it is cleaned, just as the

corroded silica glass cracks while it cools down (19). It is

pertinent here to mention that the corroded specimen needed more

than 24 hours to remove the melt penetrated inside the test pieces

whereas the corroded specimen in molten sodium tetraborate needed

only 2 to 3 hours in hot diluted HCl solution. Considering that

$NaVO_3$ is more readily soluable in diluted acid solution than

$Na_2B_4O_7$, the above penomenon may be either due to (1) the reaction

products being less soluable in acid solution or (2) Na_2O or V_2O_5

molecules may have penetrated along the grain boundaries of the

specimen where the acid solution finds difficulty in leaching. In

the latter case, penetration of the now more soluable grain boun-

daries by the hot acid solution could permit the disintegration of

the specimen into small grains.

Safdar (33) also suggests that certain constituents of the

melt, i.e. sodium and vanadium ions or Na_2O or V_2O_5 might have

penetrated along the grain boundaries of alumina while it is subjected

to molten sodium vanadate. He was able to extract Na^+ ions from

the leaching water of the corroded sapphire . He also found that the

density of the specimen corroded in sodium melts increased.

Further support is received by the fact observed by this author that the soluble material in a polycrystalline alumina specimen, held in vanadium pentoxide melt for 15 minutes at $900^{\circ}C$, could not be leached out in 48 hours in hot dilute HCl solution. As can be seen from the photograph of sectioned corroded alumina in figure 7-3, only the margin of the corroded specimen is cleaned. It may be that the vanadium which has penetrated the grain boundaries may not be so quickly leached out as that which has merely penetrated into the pores.

7-1-4 The effect of porosity of alumina on dissolution

The rate of corrosion of single crystals of alumina (sapphire) and 29% porous alumina by sodium tetraborate melt (where the diffusion controlled process is predominant as already mentioned in section 7-1-2) is shown in figure 6-5 as a function of time. The amount of corrosion of sapphire for a minute at $900^{\circ}C$, $0.0020\,gm/cm^2$ was obtained by the extension of the slope based on its parabolic nature in figure 6-1. Both curves in figure 6-5 shows that the rate of dissolution of sapphire and porous alumina is almost the same once the constant thickness of diffusion layer was built up. This phenomenon will be dealt with later.   The estimated points A and B, the junction of the dotted line, represents the amount of alumina dissolved and the time taken to build up the diffusion layer.   As clearly can be seen, the weight loss/unit area and the time taken is increased with the existance of pores. This phenomenon can easily be explained by visualizing a porous ceramic surface in contact with the melt.   The melt will be penetrating the open pores hence extra space (as much as the volume of open

pores capable of being penetrated by the melt) must be filled by saturated melt. Therefore, it will take more time and the amount of alumina dissolved will be increased. This phenomenon was also noticed by Faruqi (11) who extensively studied the corrosion of porous alumina in molten glasses.

It is considered that the actual weight loss/unit area during the formation of the diffusion layer should be less than the experimental value obtained bearing in mind that the porous specimen has in fact a larger surface area than the measured geometrical surface area. But after sufficient time has elapsed to set up the diffusion layer, the porous specimen would be dissolving at the same rate as single crystal, because the majority of the open pores are filled with the saturated melt except when the pore diameter is larger than about twice of diffusion layer thickness.

In the following diagram is shown schematically stages in the build - up of the diffusion layer until final thickness of the diffusion layer is set up.

porous refractory
surface
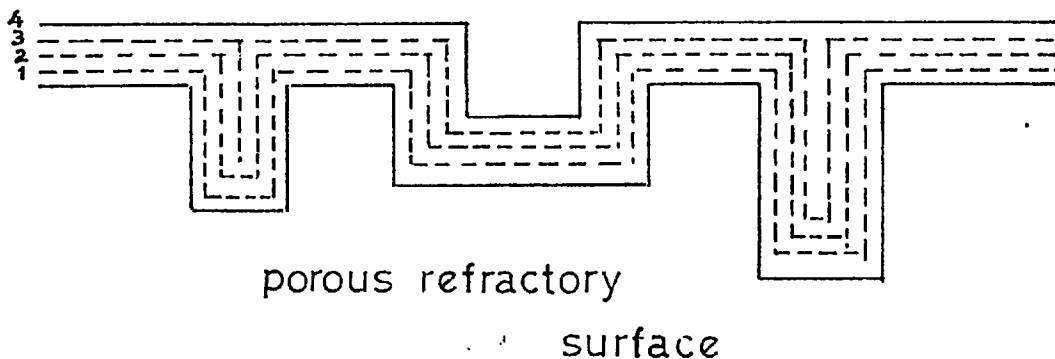
The changes of diffusion layer as time passes after the porous

alumina is submerged into the melt assuming the constant layer

thickness is completed after four minutes.

Key ; 1 — the diffusion layer after one minute

.2 — the diffusion layer after two minutes

3 — the diffusion layer after three minutes

4 — constant layer of diffusion layer

From above diagram, it is possible to make two assumptions;

(1) The pore size smaller than twice the thickness of diffusion

layer would be filled with saturated melt. Thus it wouldn't

affect the steady rate of solution.

(2) The pore size larger than twice the thickness of diffusion

layer may not be filled with saturated melt. Thus it may

increase the rate of solution.

The first assumption was already explained. The second

assumption seems supported by the observed fact on the corroded

porous alumina that the size of certain pores got larger. The

certain pores referred to here will be the pores whose size is

larger than twice the thickness of boundary layer. The photograph

of this corroded specimen is shown in figure 7-1. This reason

could also be the one of the possible explanations why the amount

of weight loss obtained by present author, was as much as twice

that obtained by Faruqi (11). The weight loss/unit area versus

time curve of 29% porous alumina is shown together with that of

36% porous alumina obtained by Faruqi in figure 6-6 and tabulated

below ;

Weight loss (gm/cm^2)

Temperature, °C	Time (min.)	Faruqi	Present results
1,000	2	0.0078	–
	4	–	0.0297
	15	0.0190	0.0395
	30	0.0286	0.0502
	Porosity	36%	29%

In constrast to the effect of porosity in diffusion controlled process, the rate of corrosion of porous alumina is increased with increase in porosity where surface – reaction is rate controlling process, i.e. alumina in molten sodium metavanadate (11). Faruqi reports that about 30% of the weight loss occured inside the pores, of which estimation was obtained by comparing the recession measurement of test pieces and the total wiehgt losses. In this connection, Barham (2) also finds the corrosion rate was increased with existence of pores of MgO in molten sodium silicate where the chemical controlled process is operative.
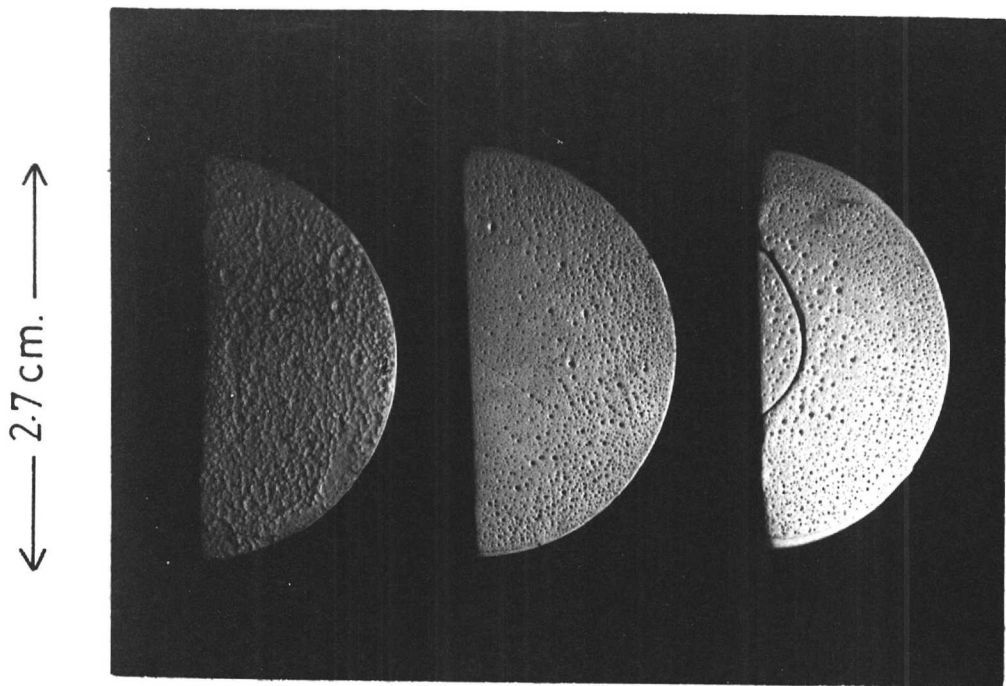
Figure 7-1 Left, carbon/alumina, one-hour in melt and then oxidised.
Middle, alumina (29% porous) immersed 30 mins..
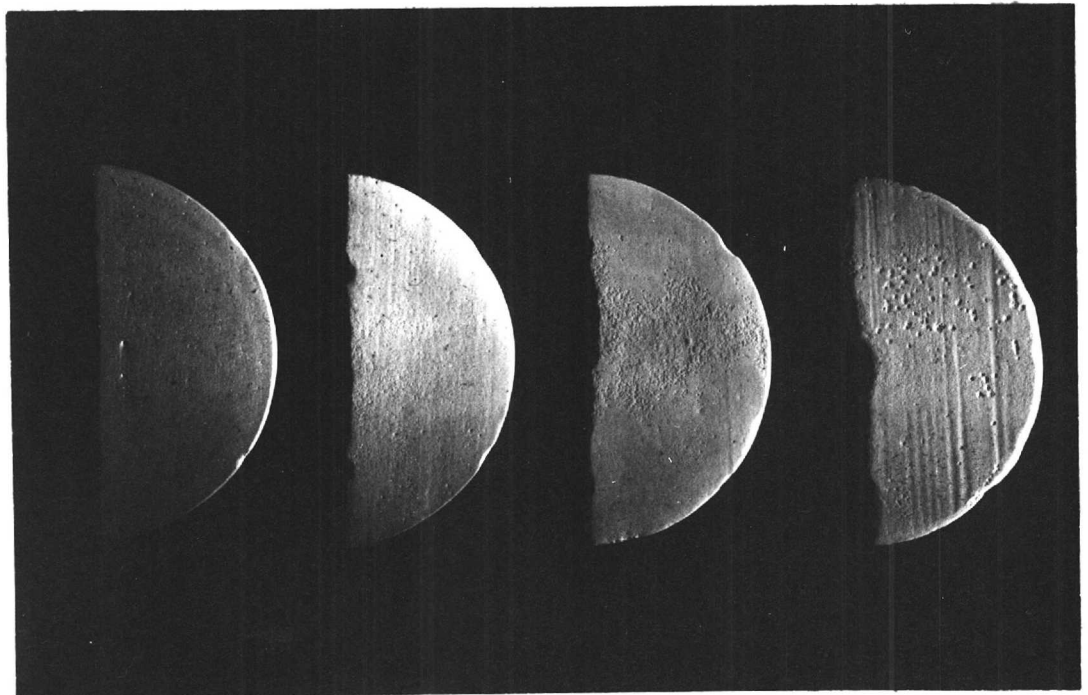Right, as 'middle' but two hours.

(All in sodium tetraborate at $1.000^{\circ}C$)

Figure 7-2 Corroded carbon-containing alumina in sodium metavanadate at $950^{\circ}C$. From left to right, immersed 4, 15, 30 and 60 mins..

7-2 The corrosion of carbon-containing alumina in sodium
tetraborate melt

The plots of weight loss/unit area versus time for the carbon-containing alumina corroding in $Na_2B_4O_7$ melt are shown in figure 6-7 to 6-9 together with those of corresponding 29% porous alumina, which doesn't contain carbon, and single crystal, i.e. sapphire. Although the values of weight loss/unit area of carbon-containing alumina are scattered partly because of experimental difficulties and the small variation of the percentage of carbon in each specimen, it reveals, first of all, the mechanism of corrosion of carbon-containing alumina is the same as alumina, i.e. the diffusion controlled process. Secondly, the rate of attack on carbon-containing alumina is decreased compared to the rate of single crystal and corresponding 29% porous alumina. Those phenomena revealed will be considered as follows.

7-2-1 The mechanism of corrosion of carbon-containing alumina
in sodium tetraborate melt.

As is well known, carbon is added to magnesite bricks to inhibit penetration of the slag into the pores when it is subjected to slag in the basic oxygen - blown steelmaking process. This is believed to be true, so long as the carbon is preserved from destructive reactions, by numerous workers (4) (16) (21), who studied slagging mechanism of carbon-bearing refractories on a laboratory scale employing real carbon-bearing magnesite or dolomite brick. If this recognition of the vital role of carbon is also applicable to the present investigation, then diminished reaction within the pores is expected where the carbon was present compared to the corresponding 29% porous alumina. This will be dealt again

in the section 7-2-2.

During the course of the corrosion experiment with carbon-containing alumina, no visible reaction between the carbon and molten sodium tetrborate with a nitrogen atmosphere above the melt, was noticed except for a few gas bubbles evolved when the first composite carbon/ alumina specimen was submerged into the melt (which was exposed in air overnight). This reaction may be supposed to be due to the oxygen dissolved in the melt and the air trapped in the pores of specimen. A few carbon particles were always noticeable in adhered melt around the corroded specimen when the specimen was released from the melt. The corroded composite specimen was covered with carbon which was held there even after the corroded specimen was cleaned in hot dilute acid solution and dried. The photograph of the carbon particles covered on the corroded specimen is shown in figure 7-4. These observations support the assumption that no reaction or negligiable reaction occured between the carbon and molten sodium tetraborate. Consequently no physical disturbance of the melt for instance by bubble release due to the reaction, where the diffusion layer is formed, is expected. Thus, this speculation leaves the rate process of corrosion of carbon-containing alumina as the same as alumina, i.e. the diffusion controlled process (31).

7-2-2   The initial corrosion rate of carbon-containing alumina

As the trend is seen in figure 6-7 to 6-9, the initial corrosion rate of carbon-containing alumina is reduced with the increasing carbon content. The phenomenon could be explained by considering that the alumina pellet became denser (less porous) by the addition of carbon, i.e. 3.7 weight % of carbon addition
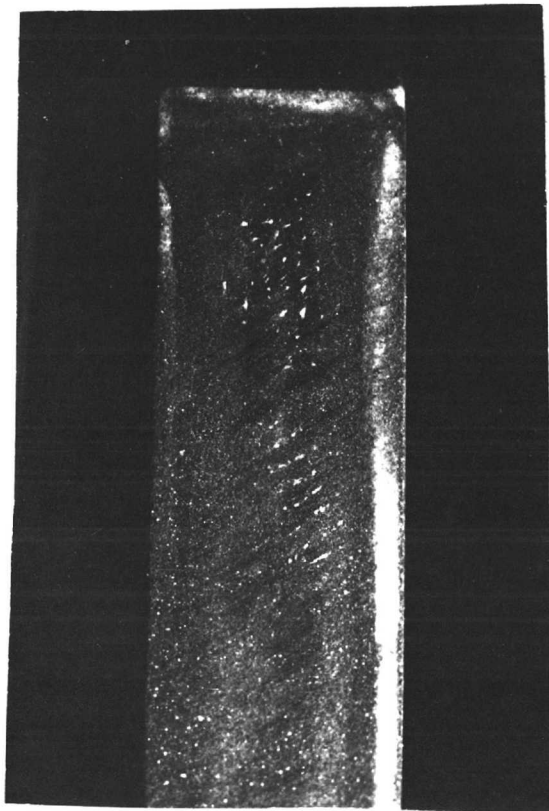
Figure 7-3 V₂O₅ had penetrated into the matrix of the polycrystalline alumina and was not leached in HCl solution for 48 hrs. except for the margin.
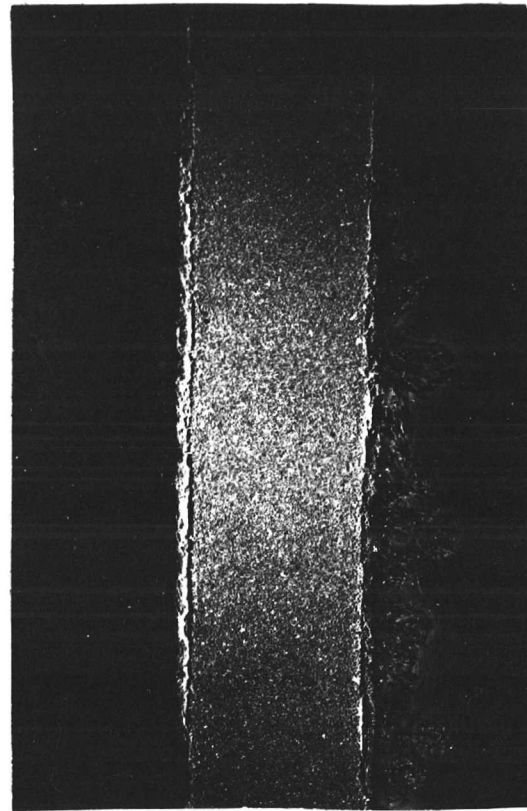
Figure 7-4 Carbon particles held on the corroded carbon-containing alumina after the corrsion by sodium tetraborate.
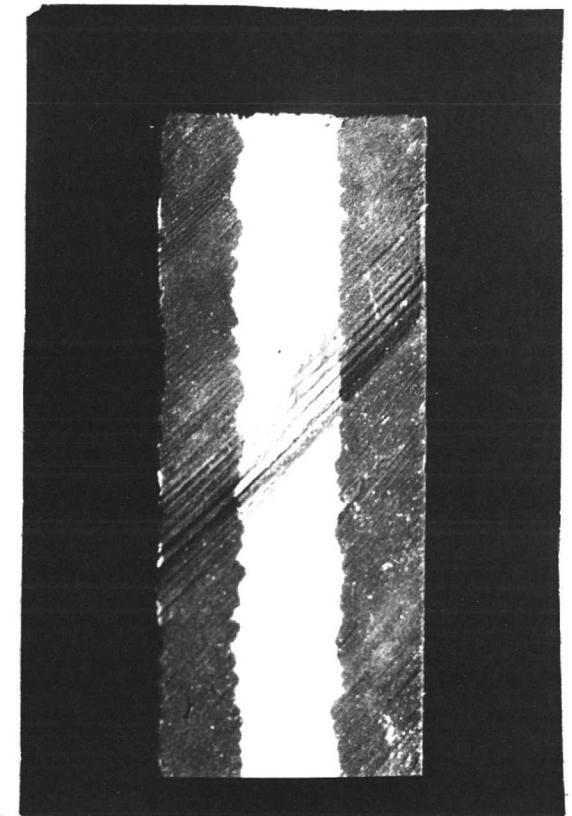
← 3.3mm. →

Figure 7-5 Top of the corroded specimen shows the melt has penetrated (sodium tetraborate) where carbon is absent but the sign of melt penetration is invisible where the carbon was present.

to the 29% porous alumina made it to act like 20% porous

alumina in the melt (this value was based on Faruqi's work-

see figure 6-14), because the carbon in the pores inhibited

the melt penetration and subsequently the pores inside have

remained in an unattacked state. Apart from the studies by

the previous workers (4) (16) (21) with good agreement,

this assumption was also reinforced by the author from the

observation made on a corroded specimen which contained carbon

only at the outer layer of the porous specimen. The outer

layer of a porous disk of sintered alumina was impregnated with

the pitch and carbonized. This specimen was then cut into half

to form half-moon shape and corroded in molten $Na_2B_4O_7$ as such

for five minutes at $900^{\circ}C$. After the adhered melt of the corroded

specimen was cleaned in hot diluted HCl solution, it was then cut

across the axis and examined under the optical microscope . The

photograph of the corroded specimen is shown in figure 7-5. As

can be seen, the melt penetrated through the pores to some distance

about 0.15 cm., where no carbon was present but no visible pene-

tration by the melt was observed where the carbon was deposited in

the pores. This observation indicated that no or, at least,

diminished space was available to accommodate the melt within the

pores where the carbon was present. This is the reverse case of

effect of porosity described in section 7-1-4. Thus, the diminished

reaction within the pores would lead to the reduced initial corrosion

rate of carbon-containing alumina.

7-2-3 The steady state corrosion rate of carbon-containing alumina

Turning now to the steady state corrosion rate of carbon-

containing alumina, of which the carbon was obtained from the

pitch, the slopes of curves were ambiguous to judge whether or not

the carbon in the pores reduced the rate of corrosion of alumina as can be seen in figure 6-7 to 6-9.   To clarify the slope of the curve better, carbon content of the composite pellets was increased up to 6.8 weight %, about 32% of pores are filled with carbon, and these pellets were submerged in the melt for up to 3 hours at 900°C.   As the curve is seen in figure 6-7, it indicated a slight tendency for the steady state corrosion rate to be reduced.   But bearing in mind that this much discrepancy was often met with in the case of both single crystal and porous alumina, this indication did not seem to stand with high degree of certainty.   But, on the other hand, the corrosion rate of carbon-containing alumina, of which the carbon was obtained from the "Cascote" resin, was reduced appreciably as shown in figure 6-8.

It is the author's opinion that if the pores of 29% porous alumina are completely blocked up with 3.6 weight % of carbon deposited from the "Cascote" resin, about 17% of pores are filled with carbon, and subsequently no dissolution occured within the pores, only alumina on the surface exposed in melt was able to react with the melt.   This surface area of alumina exposed in melt would be the measured surface area minus the area of the pores on the surface.   Then the values of weight loss/71% of geometrical surface area, assuming % of porosity is proportional to the surface area of the pores, would be similar to the weight loss/unit area values of single crystal.   Thus simple calculation was done and the values obtained are listed below together with the weight loss/unit area values of single crystal.

Carbon-containing alumina   Sapphire

| Time (min.)	wt.loss/unit area (gm/cm^2)	wt.loss/corrected area (gm/cm^2)	wt.loss/unit area (gm/cm^2)
30	0.019	0.027	0.024
60	0.026	0.036	0.036
120	0.039	0.055	0.061

As can be seen from the above table, the values of calculated weight loss and the values of weight loss of sapphire are similar. It suggests that if the carbon is blocked up the pores efficiently, the rate of solution of carbon-containing alumina is reduced because the carbon reduced the surface area as much as the area of the pores on the surface. However, the rate of solution of alumina in the carbon-containing alumina is the same as that of single crystal . It also suggests the view that even 6.8 weight % of carbon, obtained from the pitch, did not filled the pores efficiently and consequently some corrosion occured in the pores. Then the reaction may become similar to that of the porous alumina as described in section 7-1-3. It may be the explanation of why the slope of curves, shown in figure 6-7 to 6-9, of which carbon was introduced from the pitch, are similar to those of porous alumina.

7-2-4   The effect of carbon formed from pitch and "Cascote
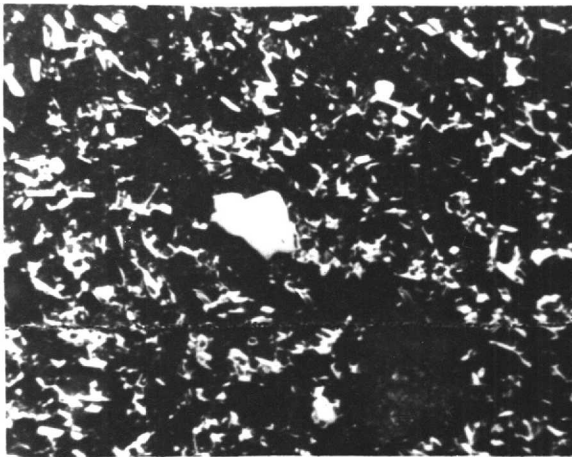
resin"

As can be seen in figure 6-8 and mentioned in section 7-2-3, it is evident that the carbon formed from the "Cascote" resin performs better than carbon deposited from the pitch. To seek possible explanation for this fact, the physical state of the pitch and "Cascote" resin while it is carbonized will be summarized first.   Briefly, the pitch turns into a viscous
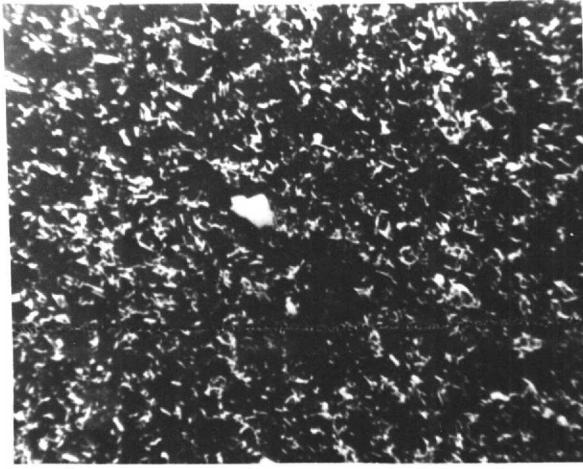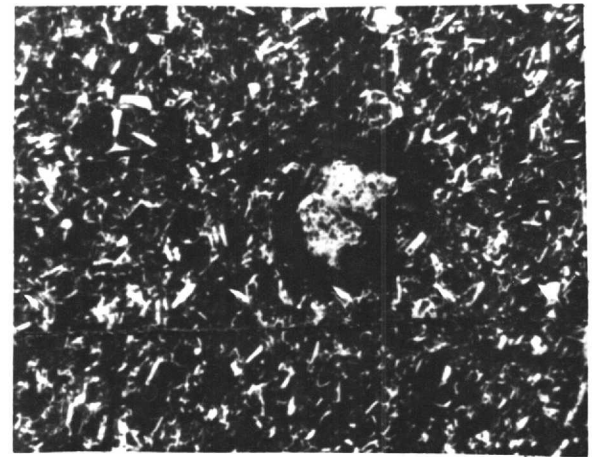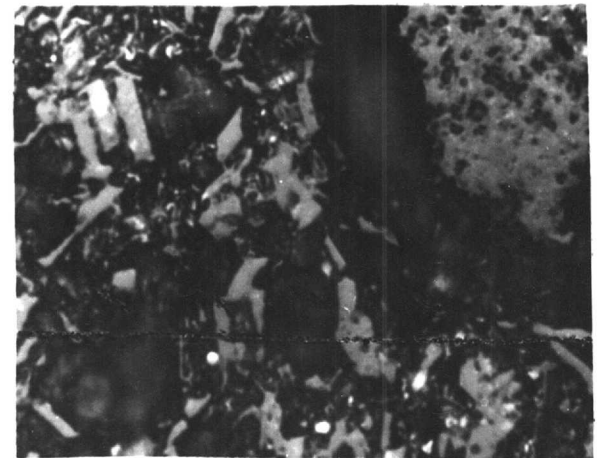
X 50 X 50
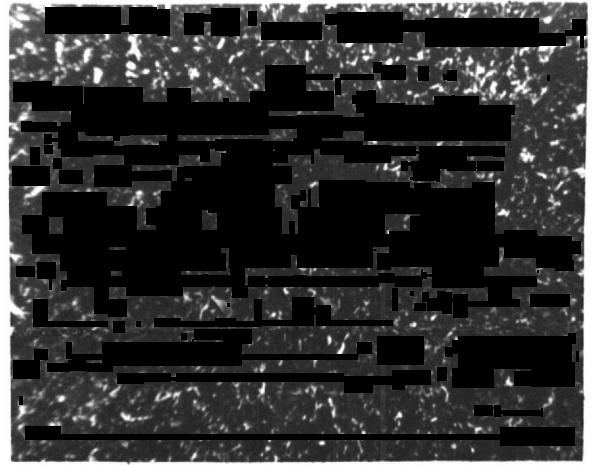
X 100 X 100

X 400 X 400

(a) (b)

Figure 7-6 Optical micrographs of carbon-containing alumina (a) 4.6 weight % of carbon deposited from pitch (b) 2.7 weight% of carbon deposited from "Cascote" resin.

liquid at 85°C and becomes less viscous before it is decomposed, giving off hydrocarbons. Then a coke residue is left. But liquid "Cascote" resin polymeries below 200°C before it is carbonized. Then the polymer decomposes directly to carbon, without passing through a liquid phase, giving off H_2O molecules first and then CO and H_2 gas at higher temperature while it is carbonized. Considering these two different phenomena, the carbon formed from "Cascote" resin may feasibly distributed in the pores of alumina uniformly whereas the carbon from the pitch might be formed in a preferred place irregularly because the pitch flowed into pores during the carbonization. Watt and Johnson (40) relate how the permeability of impregnated graphite after twelve pitch impregnation was reduced to 2.07 x 10^{-3} cm^2/sec. whereas one impregnation of porous graphite by "Cascote" resin reduced it to 2 x 10^{-6} cm^2/sec. It may be supposed that the carbon formed from the pitch was deposited in side pores or part of the wall of big pores randomly whereas the carbon formed from the "Cascote" resin may be distributed in the pores uniformly (17), having better resistance to the melt penetration compared to that of carbon formed from the pitch. The optical micrographs of carbon-containing alumina are shown in figure 7-6.

However, it must not be forgotten that the wetting characteristics and the impurities left are also important factors which has not been studied in the present work.

7-3   The corrosion of carbon-containing alumina in sodium

metavanadate melt

In contrast to the corrosion rate of carbon-containing alumina in sodium borate melt where a diffusion controlled process

prevails, unexpectedly, enchanced corrosion of carbon-containing alumina in sodium metavanadate melt occured. The values of weight loss/unit area of the composite carbon/alumina in the melt are presented in Table 6-9 and 6-10, and the plots are shown in figure 6-11 and 6-12 in comparison with those of corresponding porous alumina of 21% porosity. However, it is to be noticed that the values of weight loss/unit area of the composite specimens contain the amount of carbon oxidized due to direct reaction by $NaVO_3$. To estimate the amount of carbon retained after the composite pellet was corroded, the corroded specimens (the temperature of test was $950^{\circ}C$) were further oxidized in air at elevated temperature. By substracting the weight of carbon retained in the corroded specimen from the original weight of carbon in the composite specimen, the weight of carbon oxidized during the corrosion experiment was obtained and subsequently converted to the %. The percentages of carbon oxidized are tabulated below together with weight loss/unit area of alumina itself. The latter values were obtained by substracting the amount of carbon oxidized from the overall weight loss of the carbon/alumina composite. Also presented are the values of weight loss/unit area of corresponding 21% porous alumina.

Time (min.)	Carbon oxidized (%)	wt.loss of Carbon-containing alumina (gm/cm^2)	wt.loss of alumina itself (gm/cm^2)	wt.loss of corresponding 21% alumina (gm/cm^2)
4	23	0.0098	0.0080	0.0054
30	57	0.0490	0.0443	0.0274
60	84	0.0932	0.0886	0.0450

As can be seen from above table and the plots in figure 6-11 and 6-12, it is evident that enhanced corrosion of the composite carbon/alumina occured. The reason for enhanced corrosion is most likely to be due to the fact that carbon was highly combustible in molten sodium metavanadate, in an oxygen-free nitrogen atmosphere above the melt. The rate of oxidation of carbon in the melt is already presented in Table 5-6. Due to this oxidation, the heat evolved would have raised the temperature of the composite specimen and subsequently caused enhanced corrosion .

As is well known, carbon gets hotter than the furnace temperature when the carbon is being oxidized. Tu, Davis and Hottel (39) reported that the temperature of carbon was $70^{\circ}C$ - $110^{\circ}C$ higher than the furnace temperature when it is burned in air. No doubt, temperature of the composite carbon/alumina got higher than the temperature of melt due to the oxidation. Then the enhanced corrosion is inevitable because of raised temperature effect.

The slope of the corrosion curve of the composite carbon/ alumina, in figure 6-11, indicates that the temperature would be about $30^{\circ}C$ higher than the temperature of melt if enhanced corrosion was merely due to above mentioned effect.

Consideration was also given to various other possible reasons for enhanced corrosion, such as (1) the effect of accelerated convection of the melt due to gas release (CO and CO_2) (2) the effect of the reaction products (CO_3^{-2}) by the oxidation of carbon in the melt. However these are not likely to be vital reasons, although it needs confirmation, because (1) Faruqi (11) found that rotation of alumina rod did not increase the rate of corrosion, which

is typical confirmation of the chemical - reaction controlled

process (2) the corrosion rate of alumina in molten Na_2CO_3 is

far less than that in molten $NaVO_3$, i.e. at $1,000^{\circ}C$ 0.0011

$gm/cm^2/20$ min. for the former process and 0.0055 $gm/cm^2/20$ min.

for the latter process, respectively.

It is noticed, in figure 6-11 and 6-12, that enhanced

corrosion was greater up to 15 minutes. The explanation to

this seems to lie in the fact that more oxidation of carbon

occured when fresh melt penetrated through the pores of fresh

test piece. The percentage of carbon oxidized within the pores

of alumina in $NaVO_3$ melt is plotted in figure 6-15, as a function

of time. As can be seen, the oxidation of carbon was greater

at the first ten minutes. It supports above contention. Hence,

if the oxidation of carbon occured at a uniform rate, the degree of

enhanced corrosion would also have been uniform. It suggest the

mechanism of corrosion of the carbon/alumina is the same as alumina,

the chemical-reaction controlled process as described in section

7-1-3.

In conclusion, it can be stated that carbon in the pores of

alumina increased corrosion, due to destructive reaction between

carbon and the melt $(NaVO_3)$.

SUMMARY

The effect of carbon in carbon-containing alumina with respect to the corrosion resistance when attacked by melts, can be summarized.

I.   The effect of carbon in porous alumina, when attacked by molten sodium borate and where no destructive reaction between carbon and the melt appears to be involved, can be stated as follows : -

   (a)   when the carbon is poorly deposited in the pores, the reverse effect of porosity occurs, i.e. 3.7 weight % of carbon added to 29% porous alumina made it the equivalent of 20% porous alumina.

   (b)   when the carbon is efficiently introduced into the pores, corrosion of the carbon/alumina composite occurs below even that of sapphire. The reason for this appears to be due to the reduction of surface area by the addition of carbon.

   (c)   carbon deposited from "Cascote" resin performs better than carbon introduced from pitch.

II.   The effect of carbon in the pores of alumina when attacked by molten sodium vanadate, where direct oxidation of carbon by the melt is found, can be stated as follows : -

      enhanced corrosion of the composite carbon/alumina occurs. The most likely reason is that by the oxidation of carbon the temperature was raised above that of the melt. The effect was most noticeable in the first 15 minutes.

...

Suggestions for future work

1. The oxidation of carbon under melts has been investigated
   and the plausible explanation for the results obtained is
   given in chapter 5.   The study on the whole has shown
   interest ;   however it does raise several questions to be
   investigated for the future work.

   (a)   stirring experiment

         The formation of the carbonate rich diffusion layer

         which was postulated in section 5-4-2 , can be ascer-

         tained by this technique.

   (b)   further oxidation experiments just above the melting

         point of sodium borate and sodium vanadate.

   The change of oxidation mechanism of carbon is sodium sili-

   cate occured at $1,150^{o}C$, as shown in figure 5-4. . Hence it

   is desirable to investigate if there is also the change of

   mechanism just above the melting point of $Na_2B_4O_7$ and $NaVO_3$.

2. The corrosion of carbon-containing refractory oxide, in

   silicate melt at the wide temperature range of $1,200-1,500^{o}C$

   is suggested for the future work.

3. The corrosion of carbon-containing magnesia refractories by

   the melts at the elevated temperatures (i.e. $1,400^{o}C-1,600^{o}C$)

   where the magnesia is incompatible with the carbon, is also

   suggested.   The corrosion resistance could be measured in

   terms of the penetration depth by melts employing carbon-

   containing MgO crucible.   See for example work by Green (44).

References

1. A.S.T.M., Fink Index, P.113, 1967

2. D. Barham, Ph.D. Thesis, University of London, 1964

3. L.R. Barrett, Research, 6, 61, 1953

4. H. Barthel, Stahl Eisen, Abstract 86 (2), 81-88, 1966

5. H. Barthel, Ber. Deutch. Keram. Ges., 47 (7),402-407. 1970

6. J.H. Chesters, Iron and Steel Inst., Spec. Rep. 74,

    Discussion, P.26, 1962

7. P.W. Clark and J. White, Trans. Brit. Ceram. Soc., 49,

    305, 1949 - 50.

8. J.E. Comefero and R.K. Harsh, J. Amer. Ceram. Soc.,

    35, 130 - 134, 1952

9. A.E. Dodd and A.T. Green, Iron and Steel Inst., Spec.

    Rep. 26, 127, 1939

10. F.A. Essenhigh, R. Froberg and J.B. Howard, Ind. Eng.

    Chem., 57, 33 - 43, 1965

11. F.A. Faruqi, Ph.D. Thesis, University of London, 1960

12. M.A. Field, D.W. Gill, B.B. Morgan and P.G.W. Hawksley,

    "Combustion of pulverised coal", P.336,

    B.C.U.R.A., 1967

13. W.A. Ford, "The effect of heat on ceramics," P.171,

    Maclaren and Sons Ltd., 1967

14. W.A. Ford, Refractories J., 44 (4), 110, 1968

15. L.W. Graham, J.G. Campbell and D.R. Perels, "Nuclear

    Graphite", P.135, O.E.E.C., Dragon

    Project Symposium, Bournemouth 1959.

16. R.H. Herror, C.R. Beechan and R.C. Padfield, Amer.

    Ceram. Soc. Bull., 46, 1163, 1967

17. R.H. Herron and E.J. Runk, Amer. Ceram. Soc. Bull.,
     $\underline{48}$, 1048-1052, 1969

18. B. Hill, Ph.D. Thesis, University of London, 1963

19. J. Hlaváč and P. Strand, Silikaty, $\underline{5}$, 302, 1961

20. D.H. Hubble, Amer. Ceram. Soc. Bull., $\underline{47}$ (2), 170 1968

21. D.H. Hubble and K.K. Kappmeyer, Amer. Ceram. Soc. Bull.,
     $\underline{45}$, (7), 646, 1966

22. G.J. Janz, Molten Salts Handbook, P.55, Academic Press,
     1967

23. K.K. Kappmeyer and D.H. Hubble, "High temperature oxides",
     Part 1, P.1, Academic Press, 1970

24. J.D. Mackenzie, Chem. Rev., $\underline{56}$, 455, 1956

25. K.J.D. Mackenzie, J. Brit. Ceram. Soc., $\underline{5}$, (2), 183, 1968

26. N. McCallum, Ph.D. Thesis, University of London, 1950

27. H. Ohba, T. Ikenoue and Y. Nishikawa, Iron and Steel Inst.,
     Spec. Rep. 26, 55, 1962

28. V. Philopoulos, M.Phil. Thesis, University of London, 1964

29. G.D. Pickering and J.D. Batchelor, Amer. Ceram. Soc. Bull.,
     $\underline{50}$, (7), 611-614, 1971

30. L. Reed, Ph.D. Thesis, University of London, 1952

31. L. Reed and L.R. Barrett, Trans. Brit. Ceram. Soc., $\underline{54}$,
     671, 1955

32. P.C. Robinson, Refractories J., $\underline{42}$ (6), 218-22, 1966

33. M. Safdar, Ph.D. Thesis, University of London, 1961

34. J.A. Sharp, Private communication from the British Coal
     Tar Research Association.

35. L. Shartsis, W. Capps and S. Spinner, J. Amer. Ceram.
     Soc., $\underline{36}$, 35, 1953

36.   E.S.D. Smith, D.C.T. Thesis, Battersea College of

Technology, 1966

37.   J.E. Stanworth, "Physical properties of glass", P.14,

1953

38.   H. Towers, Trans. Brit. Ceram. Soc., 53, 180, 1954

39.   C.M. Tu, H. Davis and H.C. Hottel, Ind. Eng. Chem.,

26 (7), 749, 1934

40.   W. Watt and W. Johnson, "Nuclear Graphite" P.101,

O.E.E.C., Dragon Project Symposium,

Bournemouth 1959

41.   A.E.R. Westman, J. Amer. Ceram. Soc., 9, 311, 1926

42.   J. White, Iron and Steel Inst., Spec. Rep. 74,

Discussion, P.26, 1962

43.   J.L. White, Ph.D. Thesis, University of London, 1955

44.   J. Green, "The effect of microstructure on the

penetration of fluxes into MgO- based

bodies at high temperatures", M.Sc.Tech.

Thesis,University of Sheffield, 1971